




Design, prototyping and tests of a rollable ramp for temporary use

ELVAN DOĞAN KUMTEPE^{1,2} and GÖKHAN KIPER^{1,*} 

¹Department of Mechanical Engineering, İzmir Institute of Technology, İzmir, Turkey

²Present Address: New Jersey Institute of Technology, Newark, NJ, USA
e-mail: elvandogan@hotmail.com.tr; gokhankiper@iyte.edu.tr

MS received 11 June 2021; revised 3 September 2021; accepted 28 September 2021

Abstract. Portable ramps, used generally by wheelchair users, offer temporary solution to increase accessibility and mobility. Preferably these ramps should be compact and lightweight for ease of handling and storage. Different types of portable ramps in the market that are used by wheelchair users are generally made of aluminum and require several improvements, especially in terms of lightweight and compactness. Based on wheelchair users' inclinations a compact and lightweight rollable ramp is designed in this study. A parametric model of the links of the ramp are derived and the rolled geometry is optimized using convex hull and smallest enclosing circle algorithms. The side bars of the links are designed and manufactured from aluminum and the load-bearing panels are manufactured from sandwich composite structures with honeycomb core. Strength calculations are performed analytically and also with finite-element analysis. After the design is finalized, a prototype is manufactured. The designed ramp is 15.4% more compact and has 18.9% less weight compared to the best rival product available in the market. Load tests and functional tests are performed with voluntary wheelchair users. Several positive feedbacks are received from the participants about the ramp being practical, easy to use and store, lightweight, advantage of the anti-slip surface.

Keywords. Deployable structures; rollable ramps; wheelchair users.

1. Introduction

The term accessibility refers to products and/or services which are specifically designed for people with disabilities to provide equal accesses with people who have no disability. Although the term directly refers to disabled people, the overall benefits of increased accessibility may affect positively everyone. The increasing mobility in the globalized world, has led to need of accessibility for wheelchair users. The main objective of this study is to design a light and compact deployable ramp which offers temporary solution to increase accessibility for wheelchair users for accessing through a blank or elevated ground, or to get on a vehicle as an alternative to systems such as the one illustrated by Matsuoka *et al* [1]. Deployable ramps can be categorized into four main types according to their deployment method as telescopic, rollable, foldable and scissors (figure 1).

Telescopic structures consist of hollow cross-sectional profiles that slide into another member to achieve deployment. This type of ramps can be categorized under the title of telescopic ramps. Rollable ramps consist of serial chain members which are able to rotate about the connection axes. Thus, they can be rolled out like carpet on one side

and carry load on the other side due to the constructional design of the load-bearing members with mechanical motion limits. Foldable ramps generally consist of hinges and load-bearing panels (figure 2). These two main members provide jack-knife-like deployment. Scissor types of ramps consist of scissor members to achieve deployment. Somehow, there is only one patented example was found in the literature and have no real-life product in the market.

This paper focusses on design of a compact and lightweight rollable type ramp. Section 2 presents the conceptual design that starts with implementation of design thinking approach to the selected problem to reduce development time and uncover the user expectations. Section 3 gives brief information about detailed design process, which includes geometric and strength calculations. Moreover, CAD models of alternative designs are presented. Section 4 comprises prototyping and testing steps of the study. Finally, section 5 presents conclusions and evaluation of the success of the final assembly.

2. Conceptual design

The details of conceptual design of the deployable ramp are presented by Doğan Kumtepe *et al* [13]. In this section, the conceptual design studies are briefly

*For correspondence

| TELESCOPIC | ROLLABLE | FOLDABLE | SCISSORS |
|---|---|---|------------------------------------|
| | | | |
| U.S. Patent No. 20,130,028,693 A1, 2013 | U.S. Patent No. 7,958,586 B1, 2011 | U.S. Patent No. 20,020,108,190 A1, 2002 | Patent No. 20,110,072,596 A1, 2011 |
| U.S. Patent No. US5813071 A, 1998 | U.S. Patent No. 20,060,214,456 A1, 2006 | U.S. Patent No. 20,090,300,860 A1, 2009 | |
| U.S. Patent No. US5312149, 1994 | U.S. Patent No. 6,643,878 B2, 2003 | U.S. Patent No. 6,378,927 B1, 2002 | |
| | Patent No. 20,020,088,065 A1, 2003 | | |

Figure 1. Categorization of deployable ramps and some sample patents [2–13].



Figure 2. Conceptual design.

mentioned for the completeness of the study. Conceptual design is not only performed for determining feasible design alternatives, but also for investigating potential users’ inclinations. First of all, problem definition has been clarified by focusing on a specific target group for which design parameters, constraints and design challenges are determined. In order to achieve this aim, design thinking approach is adopted to simplify the complexity, and also to reduce the development time. Another reason for this selection is that, design thinking, which can fit almost all design or problem-solving cases, is a holistic approach and one of the core ideas of design research developed in recent years.

The first step is understanding the design challenge which the designer should understand, define and frame the problem before what appropriate solutions might be like.

According to World Health Organization (WHO), about 10% of the global population have disabilities and 10% of these require a wheelchair [14]. Moreover, several researches reveal that the majority of wheelchair users face with accessibility problems constantly in their daily lives [15–18]. Following step is observing that designer should observe how people behave and try to develop sense of empathy with possible users thereby, it creates awareness to better understand the difference between looking and seeing [19, 20]. In this context, great number of problems was observed with respect to what kind of difficulties wheelchair users get in their daily life routine in terms of accessibility. These difficulties can be listed as historical buildings, public spaces (banks, hospitals, etc.), public transportation, residences, road repairmen and cable or pipe installation (excavation works).

In the define step, semi-structured face to face interviews were conducted to uncover users’ inclinations and expectations [21]. According to users’ responses, the main problems are as follows:

- The narrowness of the apartment entrance to locate a fixed ramp (blocking the entrance and stairs permanently).
- The lack of the necessary distance to provide the appropriate angle of inclination for a wheelchair user.

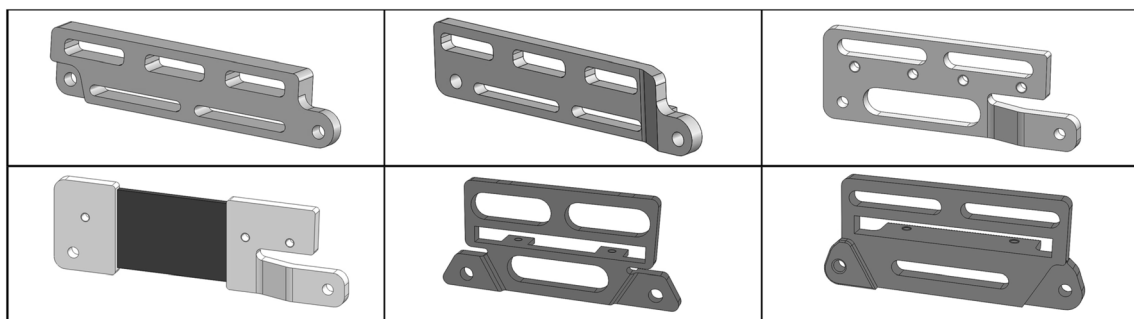


Figure 3. Alternatives for side bars.

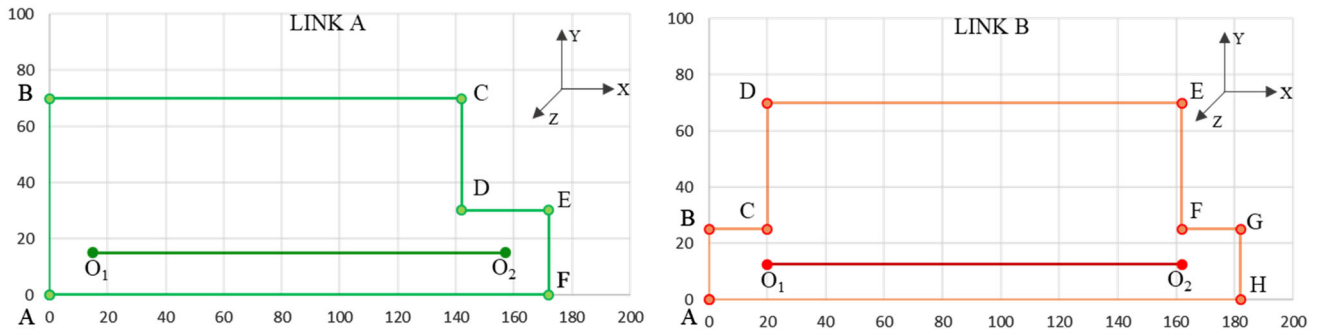


Figure 4. Asymmetrical and symmetrical link patterns.

- Being faced with some problems with their neighbors (for some functional and/or aesthetic reasons).

Ideate step provides a guideline for decision making process which can be considered as one of the most fundamental part of the conceptual design. A morphologic chart is created to reveal possible design solutions. Finally, a scaled rollable ramp is modelled (figure 2) according to the users' inclinations. The deployable ramp is designed with links which are connected to each other on the side faces. The links can rotate about the pin connections to form a rolled and a deployed configuration.

3. Mechanical design

This section comprises geometric calculations, kinematic analysis, material selection and strength calculations for the design. First, different link geometries which can provide deployment are modelled using SolidWorks.

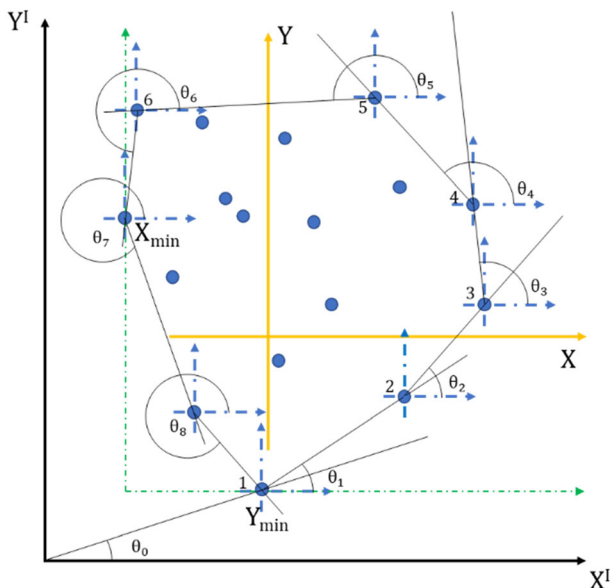


Figure 5. Illustration of the convex hull algorithm.

Then, kinematic analysis is conducted for observing compactness by using convex hull and smallest enclosing circle algorithm. Materials to be used and the manufacturing methods are determined after deciding on the link geometry. Moreover, sandwich composite plates are tested in terms of flexural behavior of the material. Design iterations are performed by conducting strength analysis, kinematic analysis and geometric calculations simultaneously by changing design parameters such as link length, height and thickness.

3.1 Geometric calculations

Geometric calculations have been conducted for achieving better compactness while the ramp is in rolled position. In accordance with this purpose, several geometric patterns of ramp links have been modelled both in SolidWorks (figure 3) and Excel with the help of convex hull and smallest enclosing circle algorithms to find feasible link lengths and shape.

Before beginning with the kinematic analysis, link alternatives have been 3D printed and evaluated in terms of manufacturability, and ease of assembly (design for assembly).

3.1.1 Kinematic analysis and design At the beginning of the kinematic analysis, two different type of side bar links were designed. 5 to 10 identical links are assembled per meter, where the link length depends on number of links per meter. Link A has an asymmetrical shape, whereas Link B has a symmetrical shape. Although the side bars have out-of-plane portions as depicted in figure 3, they are modelled and analyzed as planar geometries for kinematic analysis as shown in figure 4.

With the simplified geometry of the links, the simple kinematic chain model in Excel can be monitored at any instant. Using spin buttons of Excel, it is easy to vary the link parameters, such as $|O_1O_2| = |DE|$, $|AB| = |GH|$, $|BC| = |FG|$, $|CD| = |EF|$ and maximum allowable angles between

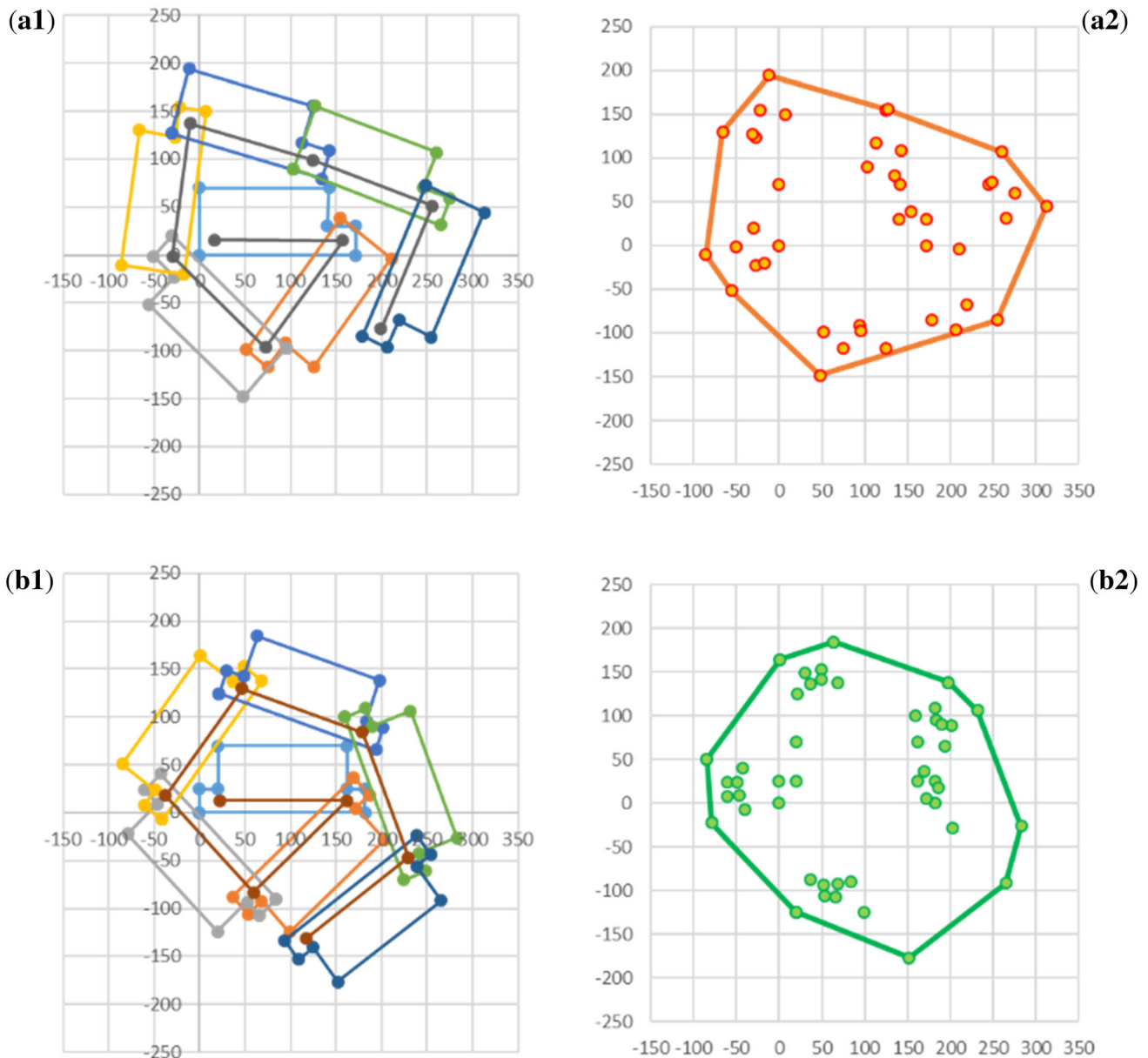


Figure 6. Convex hull of the links.

consecutive links in order to have a visual of rolled form of the ramp. This is a simple, fast and effective model for design iterations. It is also possible to pose this problem as a formal optimization problem, but constructing the model would be time consuming and the necessary software or labour would cost much more.

To carry out the kinematic analysis, the link dimensions and relative angular positions of the links with respect to each other need to be known. The vertices of side bar links are defined as points named as A, B, C, etc. in the XY-plane of a coordinate system. The first link is considered stationary and the positions of each of the other sequentially attached link is defined relative to

the previous link. The position of a link with respect to the previous one is defined as a rotation by θ and a translation by x_t, y_t . The coordinate transformation of a point on a link is performed as:

$$\begin{bmatrix} \cos \theta & -\sin \theta & x_t \\ \sin \theta & \cos \theta & y_t \\ 0 & 0 & 1 \end{bmatrix} \begin{bmatrix} x \\ y \\ 1 \end{bmatrix} = \begin{bmatrix} x \cos \theta - y \sin \theta + x_t \\ x \sin \theta + y \cos \theta + y_t \\ 1 \end{bmatrix} \tag{1}$$

Let m be the distance between the rotation centers O_i and O_{i+1} of links i and $i + 1$. Then coordinates of left bottom corner of each link is computed as:

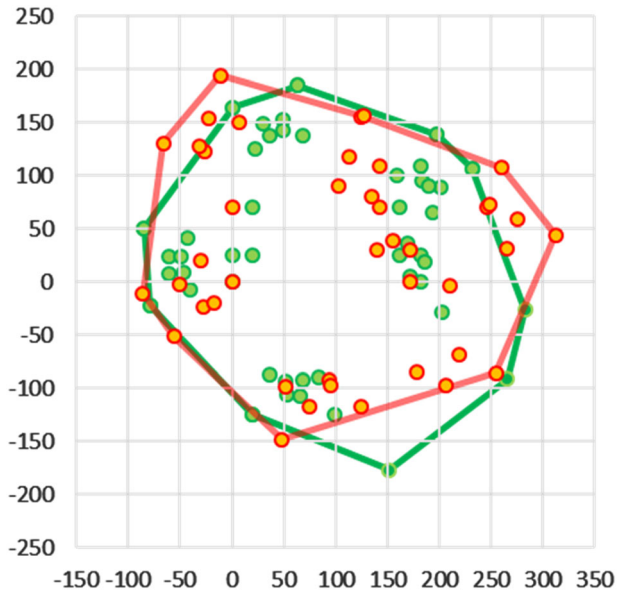


Figure 7. Comparison of the convex hulls.

$$A_{i+1,x} = O_{1x} + m + (A_{ix} - O_{1x}) \cos\left(\sum_{n=1}^i \theta_n\right) - (A_{iy} - O_{1y}) \sin\left(\sum_{n=1}^i \theta_n\right) \quad (2)$$

$$A_{i+1,y} = O_{1y} + (A_{ix} - O_{1x}) \sin\left(\sum_{n=1}^i \theta_n\right) + (A_{iy} - O_{1y}) \cos\left(\sum_{n=1}^i \theta_n\right) \quad (3)$$

The aim in the kinematic design is to select proper number of links with proper link dimensions and proper folding angles so that a ramp with a specified deployed length will roll into the most compact form. For folding analysis, one end of the serial linkage is kept fixed and the rest of the links are rolled around the fixed link. Starting with the proximal links, the angles between consecutive links are gradually increased in Excel using spin buttons until a link contacts another. After the most compact form is obtained, a convex hull algorithm is used in order to determine outer boundaries of the folded form and encircle the convex hull to get a measure for the size.

3.1.2 Convex hull algorithm Imagine that the vertices of the ramp links are nails sticking out of the plane, take a rope, wrap it around the nails until it comes back to the starting point. The area enclosed by the rope is the convex hull. “Jarvis march” or “gift-wrapping” algorithm [22] is one of the simple-minded algorithms for convex hulls of planar point clouds [23]. Let $S = \{S_1, S_2, \dots, S_n\}$ be a finite set of points in the XY-plane and X_i and Y_i be the Cartesian coordinates of the i^{th} point in the set. Then the algorithm steps are as follows:

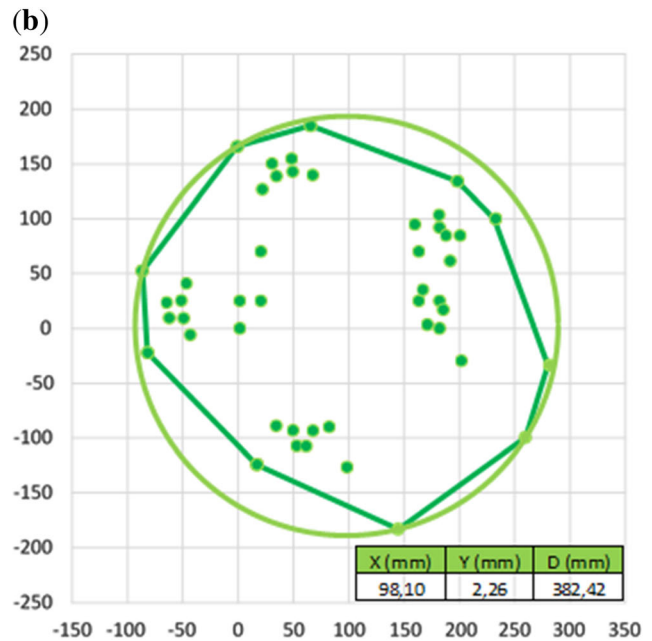
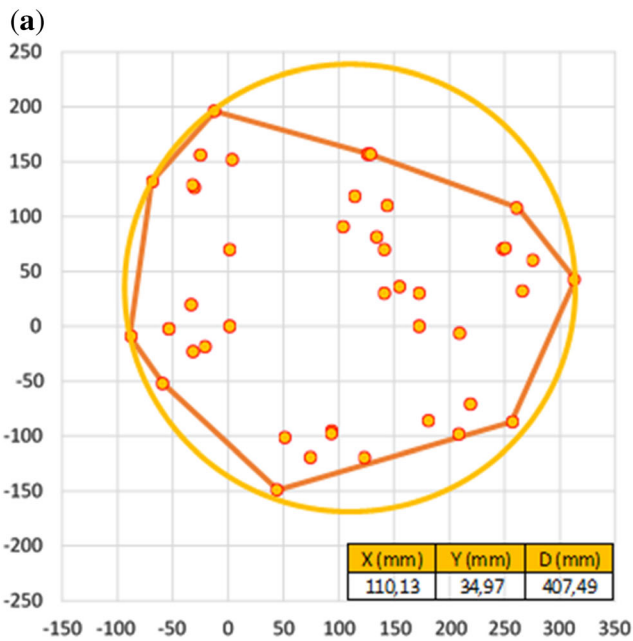


Figure 8. Smallest enclosing circle of (a) asymmetrical and (b) symmetrical links.

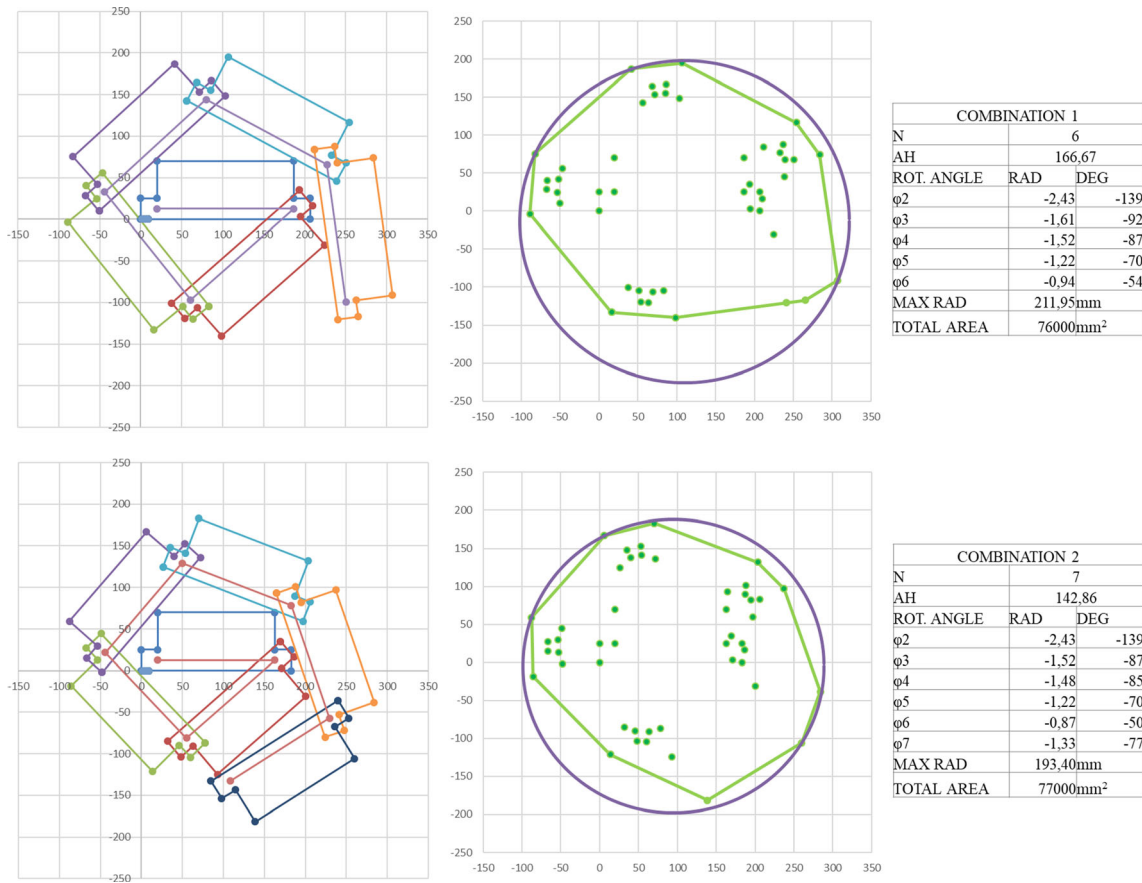


Figure 9. The effect of link length on compactness and total weight for N = 6 and 7.

Step 1. Pick an origin point outside the set (for example pick $X_{origin} \leq \min\{X_i\}$ and $Y_{origin} \leq \min\{Y_i\}$) (figure 5). Set a Cartesian reference frame at this origin.

Step 2. Find S_k such that $\theta_{0k} \leq \min\{\theta_{0i}\}$, $i = 1, 2, \dots, n$, where θ_{0i} is the angle of the position vector of point S_i with respect to the original reference frame. For equal minimum angles pick the point closest to the origin.

Step 3. Shift origin to S_k and repeat step 2 with consistent angle direction and origin until first convex hull point is re-found [23].

The convex hull algorithm is used to identify the outmost points of the point set and to plot the periphery of the ramp while it is in rolled position. Two different link shapes were modelled in Excel to observe the effects of link geometry on compactness. In the following examples, a seven-link assembly is used for a ramp with 1 m deployed length. As can be seen from figures 6-7, convex hull gives a foresight about how much space the link chains are occupying when the ramp is in rolled position. Convex hull of Link A1 looks less round due to the asymmetrical link shape, however Link B1 is designed to be symmetrical, and its convex hull looks rounder which provides more regular deployment. To observe

compactness of the links in more detail, smallest enclosing circle algorithm is used.

3.1.3 Smallest enclosing circle algorithm This algorithm can be simplified by using the convex hull algorithm to eliminate null points which are encircled in the circle. Hereby, the problem transforms into computing the smallest enclosing circle of a convex polygon [24]. This time $S = \{S_1, S_2, \dots, S_n\}$, is the finite set of vertices of a convex hull. Let $p = (x_i, y_i)$, $q = (x_j, y_j)$, $t = (x_k, y_k)$ be the three points in S which defines the smallest enclosing circle. Two of these points, say p and t , may be concurrent, in which case, the circle passes through two points $p = t$ and q which constitute the diameter of the smallest enclosing circle. A circle with center (a, b) and radius r can be expressed as

$$(x - a)^2 + (y - b)^2 = r^2 \tag{4}$$

a, b and r can be expressed in terms of the three-point coordinates as

$$\Delta = (x_i - x_j)(y_i - y_k) - (x_i - x_k)(y_i - y_j) \tag{5}$$

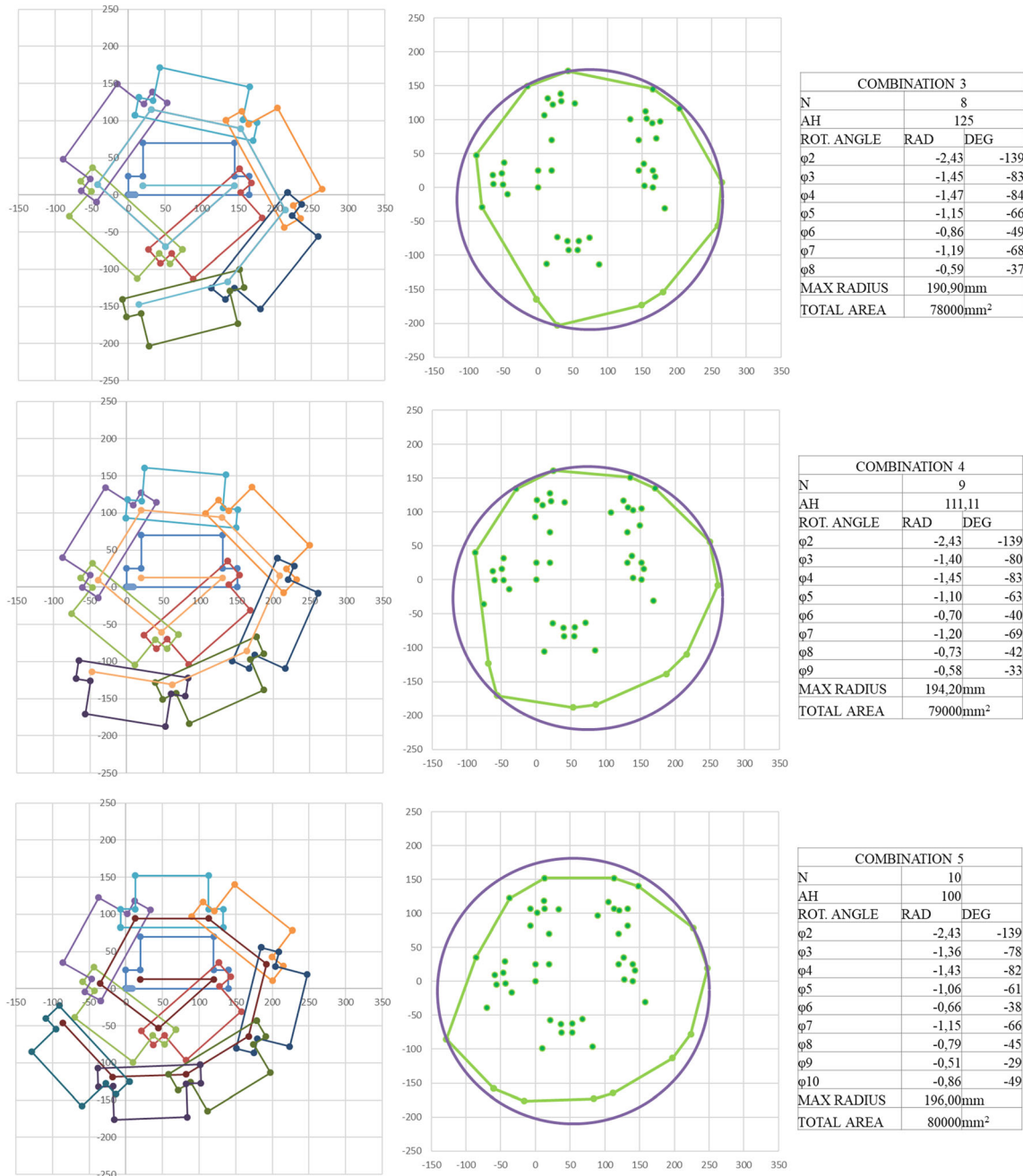


Figure 10. The effect of link length on compactness and total weight for N = 8, 9 and 10.

$$a = \frac{(x_i^2 + y_i^2 - x_j^2 + y_j^2)(y_i - y_k) - (x_i^2 + y_i^2 - x_k^2 + y_k^2)(y_i - y_j)}{2\Delta} \tag{6}$$

$$b = \frac{(x_i^2 + y_i^2 - x_k^2 + y_k^2)(y_i - y_j) - (x_i^2 + y_i^2 - x_j^2 + y_j^2)(y_i - y_k)}{2\Delta} \tag{7}$$

$$r = \sqrt{(x_i - a)^2 + (y_i - b)^2} \tag{8}$$

The smallest enclosing circle is found by trying out all possible point combinations in S for $i = 1, \dots, n$, $j = i + 1, \dots, n$ and $k = j + 1, \dots, n$, where n is the number of convex hull points.

3.1.3.1. The effect of link geometry on compactness

Two different link shapes are compared with each other to observe the effect of link geometry on compactness. After serial trials, the angle between the first two links in the

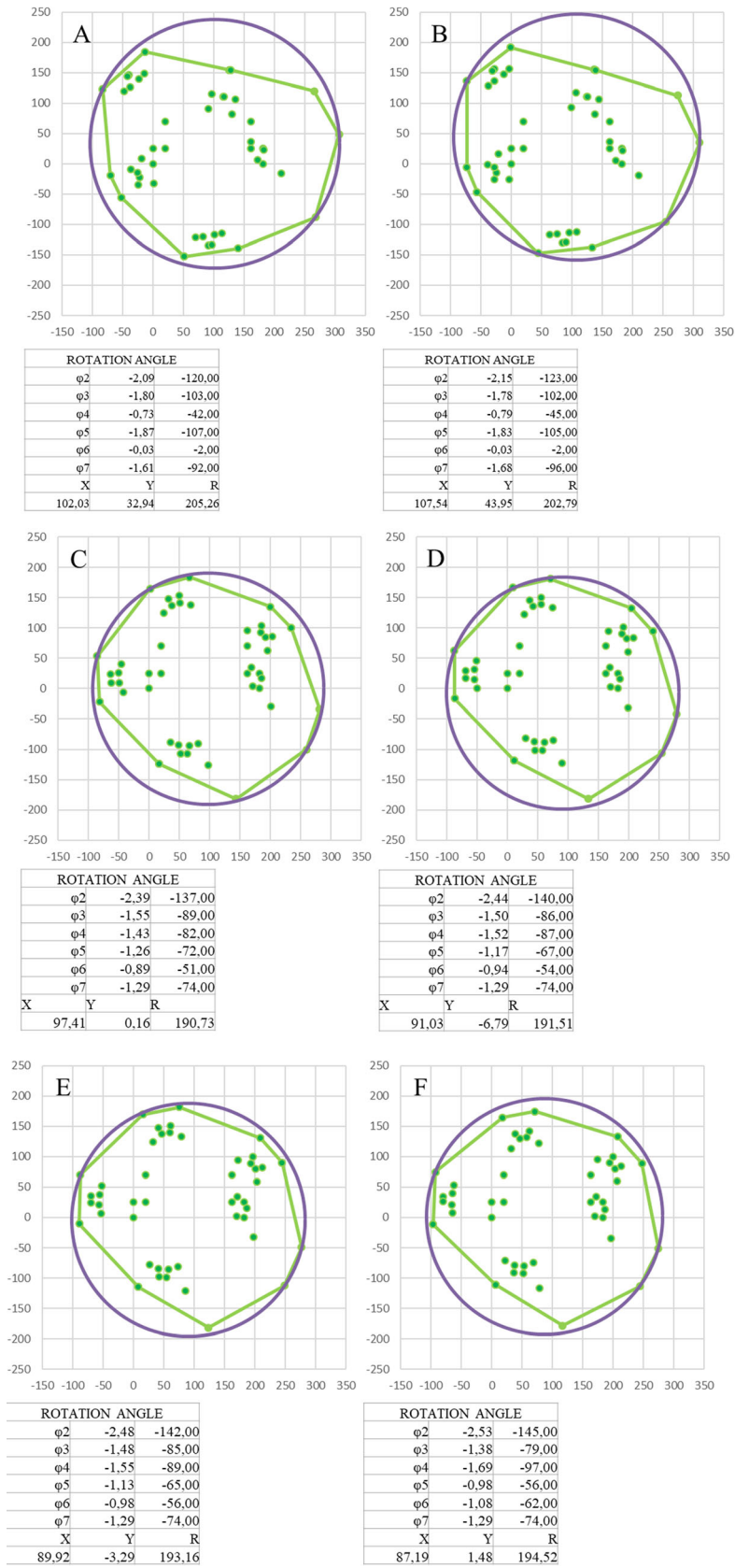


Figure 11. Effect of the rotation angle on compactness - 120°, 123°, 137°, 140°, 142°, 145° cases.

Table 1. Mechanical properties of Al 7075-T6 and Al 6061-T6.

| | 7075-T6 | 6061-T6 |
|---------------------------|----------|----------|
| Ultimate Tensile Strength | 572 MPa | 310 MPa |
| Tensile Yield Strength | 503 MPa | 276 MPa |
| Modulus of Elasticity | 71.7 GPa | 68.9 GPa |
| Poisson’s Ratio | 0.33 | 0.33 |
| Fatigue Strength | 159 MPa | 96.5 MPa |
| Shear Modulus | 26.9 GPa | 26 GPa |
| Shear Strength | 331 MPa | 207 MPa |

rolled form is chosen as 139° and all the other rotation angles are increased until the links interfere with other links. As illustrated in figure 8, symmetrical link shape is more effective in terms of rolling capability.

3.1.3.2. The effect of link length on compactness and total weight

6 to 10 identical symmetrical links are assembled for a 1 m ramp to observe the effect of link length on the compactness and total weight where the link length (DE) depends on number of links (N) per meter while the other parameters remain constant. The angle between the first two links is chosen as 139° and all other rotation angles are increased until the links interfere with other links. Total link weight per meter is proportional to the total area of the link while the thickness remains constant. Results for N = 6, 7, 8, 9 and 10 are illustrated in Figures 9-10.

Although the smallest enclosing circle forms for N = 8, total link weight is larger than the case with N = 7 and the radii are close to each other. Therefore, considering both compactness and lightweight, N is selected as 7.

3.1.3.3. The effect of rotation angle on compactness

Another design parameter that has a significant effect on compactness is rotation angle between first two consecutive links. To determine the optimum rolling ability,

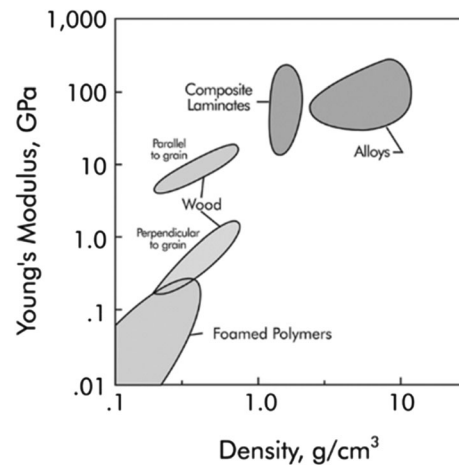


Figure 13. Modulus-density chart for various classes of materials [31].

compactness is observed by changing first rotation angle from 120° to 145°. Some of the results are illustrated in figure 11. The maximum compactness is obtained when the angle between the first two consecutive links is 137°.

3.2 Manufacturing method and material selection

One of the most important design steps is selection of strong and light-weight materials for the ramp. Manufacturing methods and materials must be selected by taking into consideration that the ramp has two main parts which are side bars and panels. Side bars are designed to form two parallel serial chains and rotate about their pivot points to be able to roll. On the other hand, the panels are designed to be attached in between two side bars to transfer the wheelchair user throughout the ramp.

3.2.1 Side bars Side bar geometry is modeled to constitute a self-standing assembly while the ramp is in deployed position. Materials with low density and high

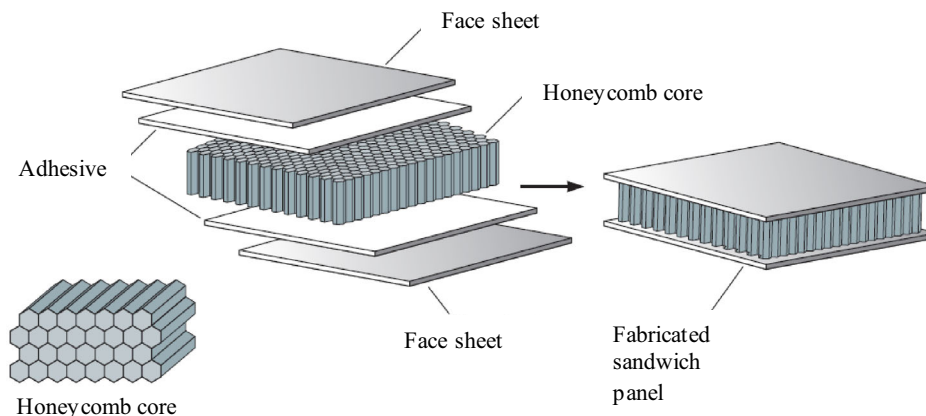


Figure 12. Sandwich composite structure [25].

strength-to-weight ratio should be used. Although, the first thing that comes to mind is using composite materials due to lightness, manufacturing cost is quite high due to complicated link shape.

Aluminum is a conventional lightweight material with density of approximately one-third of the density of steel. Aluminum alloys have low tensile properties compared with steel and their specific strength (or strength-to-weight ratio) is quite outstanding [25–28].

For material selection, two different types of aluminum alloys are compared due to their mechanical properties (table 1) and material cost. Although, 7075-T6 is one of the strongest aluminum alloys in the market and used widely in aerospace industry, its high price, embrittlement, lower corrosion resistance and tougher machinability should be taken into account. On the other hand, 6061-T6 is one of the commonly used strongest alloys in 6XXX series and it has lower price compared to 7075-T6. Material selection step is conducted simultaneously with the strength calculation step by comparing the structure's factor of safety.

The manufacturing method selection can be done properly according to design parameters and selected material characteristics. The most effective manufacturing method for building a prototype with aluminum is machining due to material characteristics and budget constraint.

3.2.2 Load-bearing panels The conceptual shape of load-bearing panels are much more simple compared to side bars, so composite materials can be used. Although, both raw materials and manufacturing methods of composite materials are costly, it is possible to reduce the total cost of composite panels by using core materials like foam, kraft paper and/or honeycomb structures. Sandwich panels (figure 12) typically consist of two thin face sheets which are adhesively bonded to a lightweight thicker core [25, 29].

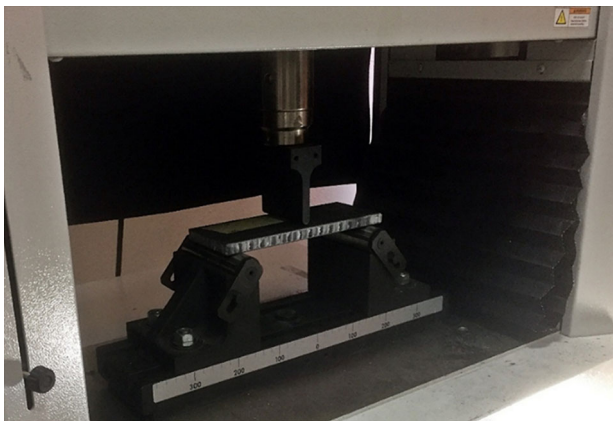


Figure 14. Three-point bending test.

Determination of mechanical properties of a sandwich composite structure's face sheets and core materials is crucially important for analysis and design. It is possible to find mechanical properties of conventional materials, especially metals, in textbooks on materials science and strength of materials [25, 30, 31]. However, composite materials contain large variety of fibers, matrix materials (epoxy, polyester, etc.) and different fiber orientations make mechanical test a necessity to determine the mechanical properties of them [29]. The materials property charts in [31] can guide to select face and core materials (figure 13). Face sheets are generally made of composite laminates and light-weight alloys with high modulus, while cores with lower density are formed of thicker metallic and non-metallic honeycombs, foams, balsa wood or trusses [32].

Using the chart in figure 13, sandwich beams are fabricated by bonding twill-woven 245 g/m² carbon fiber fabric/epoxy resin face sheets to polypropylene, aluminum, kraft paper honeycomb and Airex® foam cores with an epoxy adhesive. After producing the samples, it is decided that panels with PP and Al honeycomb core should be subjected to flexural test. Panels with kraft paper honeycomb and Airex® foam core do not meet the expectation in terms of lightness and also, it is hard to find these cores with various thickness in the market. Sandwich composite panel length (ramp width) is selected as 800 mm according to a standard adult wheelchair's size. Although, there are some special designed wheelchairs with the width of 760 mm in the market, standard wheelchair width is in the range between 600 and 650 mm.

There is no known standard for portable ramps. However, there is a standard for fixed ramps called "TSE 9111-The requirements of accessibility in buildings for people with disabilities and mobility constraints". The measurements mentioned in this standard are highly extreme for a portable ramp due to users' expectation about easy transportation. However, the ramp width can be changed easily by changing the panel length according to requirements which are explained in TSE 9111.

3.2.2.1. Flexural testing procedure

Flexure tests on flat sandwich construction may be conducted to determine the sandwich flexural stiffness, the core shear strength and shear modulus, or the facing's compressive and tensile strengths. Tests to evaluate the shear strength of the core may also be used to evaluate core-to-facing bonds. This test method provides a standard method of obtaining the sandwich panel flexural strengths and stiffness.

Sandwich beams are fabricated with proper measurements, and loaded with a loading speed 2 mm/s, under three-point bending in a Shimadzu AG-IC universal testing machine according to ASTM C 393 Standard Test Method for Flexural Properties of Sandwich Constructions

Table 2. Three-point bending test results.

| Core material | Face Thickness (mm) | Panel Thickness (mm) | Core Ultimate Shear Strength (MPa) | Bending Ultimate Strength (MPa) | Panel Bending Stiffness (D) (N-mm ²) |
|---------------|---------------------|----------------------|------------------------------------|---------------------------------|--|
| Al Honeycomb | 1.26 | 12.52 | 0.505 | 37.5 | 31756226 |
| PP Honeycomb | 1.425 | 12.85 | 0.678 | 20.426 | 18242777 |

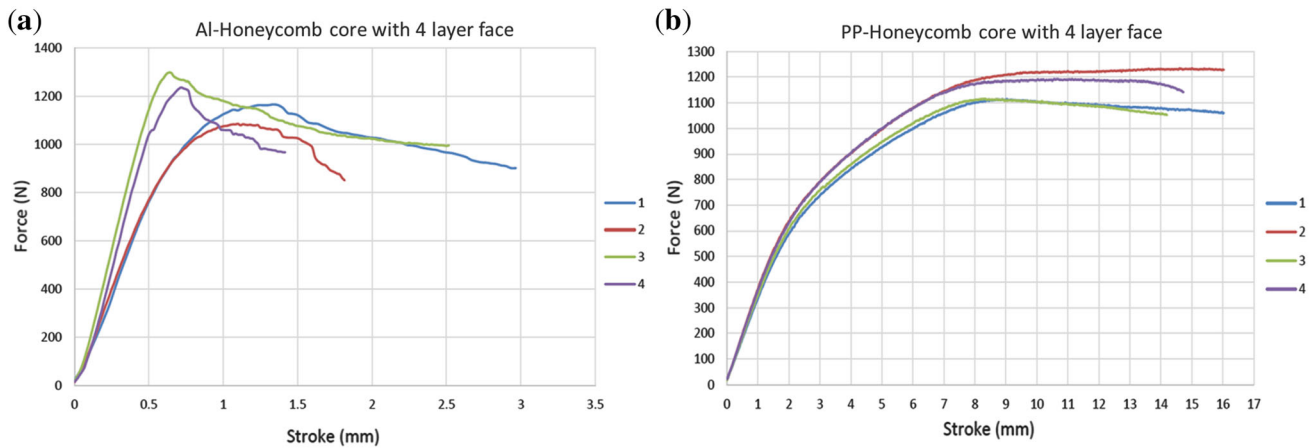


Figure 15. Force-Stroke diagram of (a) Al and (b) PP honeycomb core sandwich panels.

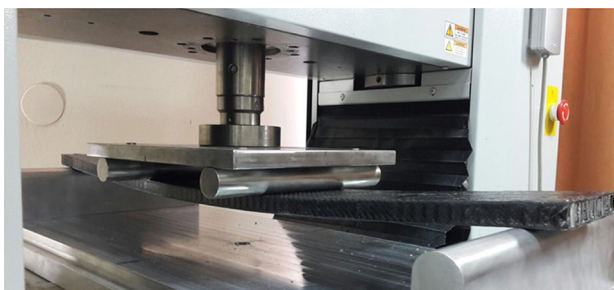


Figure 16. Four-point bending test.

(figure 14). The data sets relating the loads and the mid-span deflection of the panel specimen are automatically detected and directly recorded with a computer in real time while the stroke of the actuator advances. Test specimens are prepared according to ASTM C393 with 200 mm length

and 75 mm width and span length is selected as 150 mm. First test is conducted with 10 mm-thick PP honeycomb (0.08 g/cm³) and 10 mm-thick Al honeycomb core material with 0.034 g/cm³ density and 4 layers of twill woven carbon fiber fabric face sheets to observe the effect of different core materials on core ultimate shear and panel bending strength and stiffness (D).

First group of flexural test results (table 2) show the effects of different core materials on core ultimate shear, bending ultimate shear strength and panel bending stiffness.

The linear elastic behavior for green specimen of Al honeycomb cored sandwich panel is observed until the load approaches to about 1250 N (figure 15a), however standard deviation is relatively high and results can be considered inconsistent compared to figure 15b. Although, bending ultimate strength and panel bending stiffness of Al honeycomb cored sandwich are higher than PP honeycomb cored sandwich panel, core ultimate shear strength is lower. The

Table 3. Sandwich panel test specimens with Al honeycomb core.

| No. | Core Thickness (mm) | Face Thickness (mm) | Panel Thickness (mm) | Width (mm) | Panel Length (mm) | Support Length (mm) | Loading Span Length (mm) |
|-----|---------------------|---------------------|----------------------|------------|-------------------|---------------------|--------------------------|
| 1 | 10 | 1.425 | 12.85 | 125 | 800 | 740 | 220 |
| 2 | 15 | 1.475 | 17.95 | 125 | 800 | 740 | 220 |

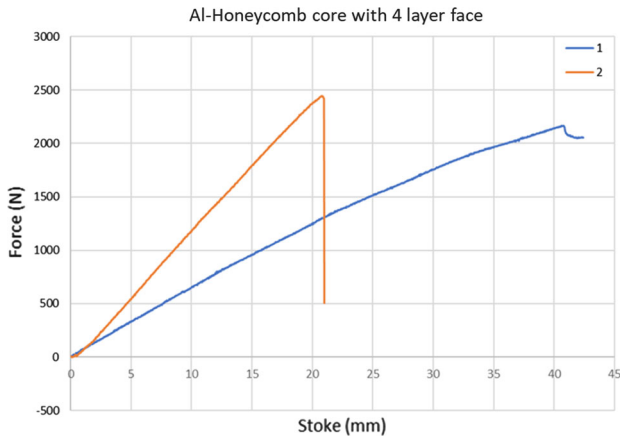


Figure 17. Force-Stroke diagram of Al honeycomb core sandwich panels.

reason of these inconsistencies for Al honeycomb cored sandwich panel may be weak bonding surface area between face and core material that causes core-skin separation. The possibility of separation between Al honeycomb core and face material may be reduced by wrapping panel with pre-preg CF face material which is basically pre-impregnated CF fabric where the epoxy is already present in the material.

Second group of flexural test is conducted with the Al honeycomb sandwich beams which are fabricated according to ramp design measurements, and loaded under four-point bending in a Shimadzu AG-IC universal testing machine according to ASTM C 393 Standard Test Method for Flexural Properties of Sandwich Constructions (figure 16). Two different test specimens are tested. Al honeycomb core with 10 mm and 15 mm-thick cored 740 mm span length, 125 mm width sandwich panel are tested with 220 mm load span length (table 3).

Figure 17 shows the new pre-preg coated sandwich panel test results which exhibit a different behavior than a

| Heavy duty products | | | |
|-----------------------|---------|-----|-----|
| Weight capacity (kgf) | 100 | 204 | 183 |
| Product weight (kgf) | 115 | 55 | 94 |
| Total weight (kgf) | 215 | 259 | 277 |
| Average (kgf) | 250,3 | | |
| Total width (mm) | 599-650 | 630 | 635 |
| Average (mm) | 628,5 | | |

Figure 19. Heavy duty products in the market [33].

classical sandwich panel (figure 15a). Face fracture occurs before core yields (figure 18). Test results can be seen in table 4. For design, 10 mm-thick cored sandwich panel is selected in terms of lightness and high bending ultimate strength. Factor of safety calculations, shear, bending moment and deflection diagrams are illustrated in section 3.3.

3.3 Strength calculations

Strength calculations are conducted by selecting a simply supported beam with certain link length, height and thickness. The beam model for the evaluations is constructed assuming a self-standing form of the ramp in deployed state thanks to the design of the links with mechanical limits to prevent further motion of the serial linkage. First, the free-body diagram of a standard wheelchair is drawn. Even though the total weight capacity of a standard wheelchair and product itself is lower than 200 kgf, there are some heavy-duty type products with total weight more than 250 kgf (figure 19).

The ramp’s load-bearing capacity is expected to be 300 kgf (2942 N) per 2 meters to prevent the possibility of user



Figure 18. Sandwich beam face fracture.

Table 4. Four-point bending test results.

| No. | Core Ultimate Shear Strength (MPa) | Bending Ultimate Strength (MPa) | Panel Bending Stiffness (D) (N·mm ²) |
|-----|------------------------------------|---------------------------------|--|
| 1 | 0.763 | 118.307 | 421603798 |
| 2 | 0.62 | 84.598 | 605753241 |

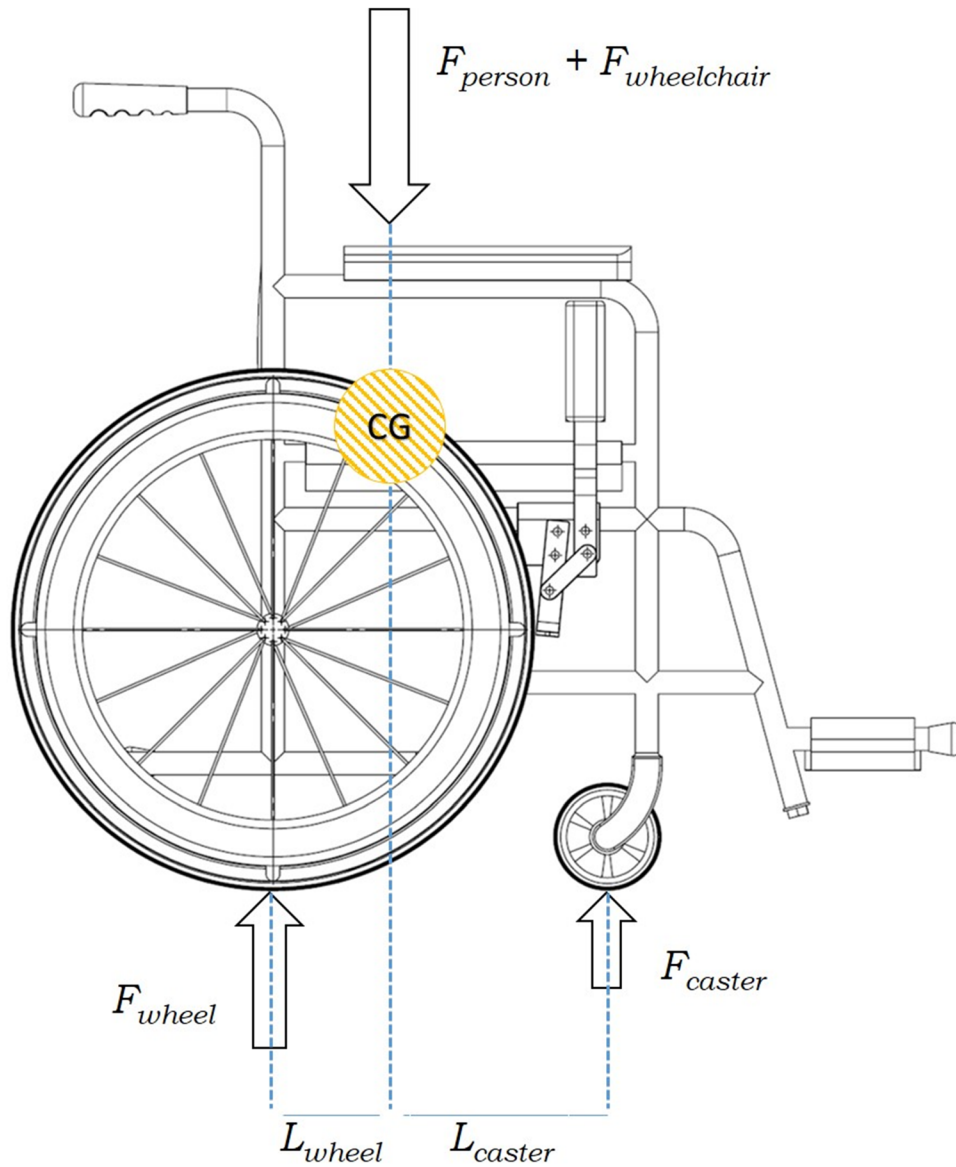


Figure 20. Free-body diagram of a wheelchair [34, 35].

error in terms of exceeding load capacity. The ramp is designed to be modular with 1-m modules which can be carried in rolled form separately and can be assembled into longer ramps with pin connections. The aim of this selection is to take extra safety precaution besides the factor of safety during structural design. The center of gravity (CG) of a wheelchair is the average location of the total weight of both user and the wheelchair (figure 20). The reaction forces at the wheels due to the wheelchair and user weight ($F_{person} + F_{wheelchair} = 2942\text{ N}$) can be computed from force and moment equilibrium equations:

$$\sum F = 2F_{wheel} + 2F_{caster} - (F_{person} + 2F_{wheelchair}) = 0 \tag{9}$$

$$\begin{aligned} \sum M_{caster} &= (F_{person} + 2F_{wheelchair})L_{caster} \\ &\quad - 2F_{wheel}(L_{caster} + L_{wheel}) \\ &= 0 \end{aligned} \tag{10}$$

$L_{caster} = 406\text{ mm}$ and $L_{wheel} = 102\text{ mm}$, so

$$F_{wheel} = \frac{(F_{person} + F_{wheelchair})(L_{caster})}{2(L_{caster} + L_{wheel})} = 1175\text{ N} \tag{11}$$

$$F_{caster} = \frac{(F_{person} + F_{wheelchair}) - 2(F_{wheel})}{2} = 296\text{ N} \tag{12}$$

A prismatic beam subjected to pure bending is bent into an arc. In case of a prismatic beam the flexural rigidity EI is constant. By integrating the governing differential equation

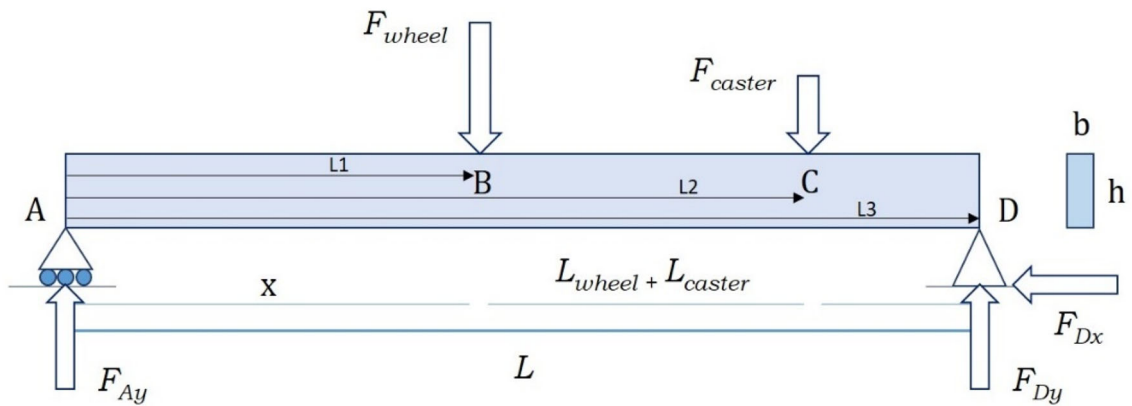


Figure 21. Determining the maximum deflection of the simply supported beam.

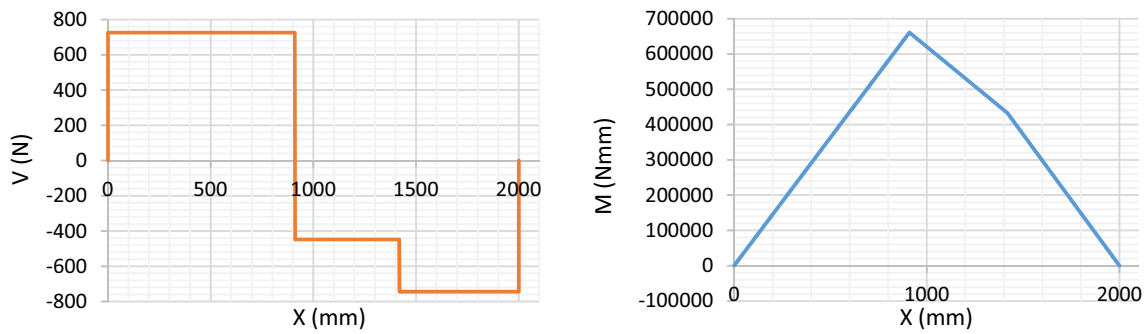


Figure 22. Shear force and bending moment diagrams

Table 5. Design parameters.

| PARAMETERS | |
|-------------------------|-------------|
| L (mm) | 2000 |
| F_{wheel} (N) | 1175 |
| F_{caster} (N) | 296 |
| X (mm) | 910 |
| BC (mm) | 508 |
| E (N/mm ²) | 68900–71700 |
| b (mm) | 10 |
| h (mm) | 70 |
| I (mm ⁴) | 285833.3333 |
| EI (N·mm ²) | 19693916667 |

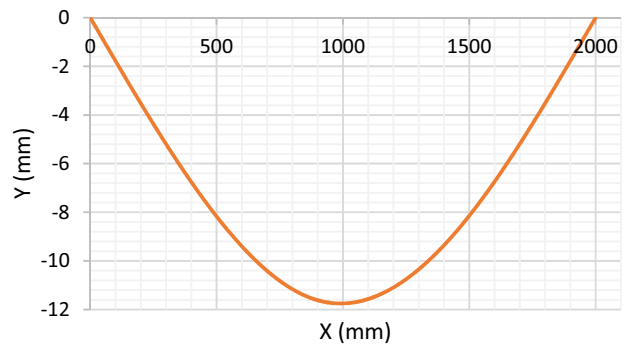


Figure 23. Deflection diagram.

for an elastic prismatic beam curve, the amount of deflection, y , can be found from

$$EIy = \int_0^x \left[\int_0^x M(x)dx \right] dx + C_1x + C_2 \quad (13)$$

where the integration constants C_1 and C_2 are determined from the boundary conditions or, more precisely, from the conditions imposed on the beam by its supports [30]. A

simply supported beam is modelled according to transverse loading conditions of the free-body diagram of a wheelchair to find numerical and analytical solution with the help of singularity function. The reason of this calculation is determining where the maximum deflection occurs throughout the ramp and the factor of safety for conducting structural design. In the case of a beam loaded with a uniformly distributed load, the shear force and bending moment can be represented by continuous analytical functions. However, in the case of a simply supported beam

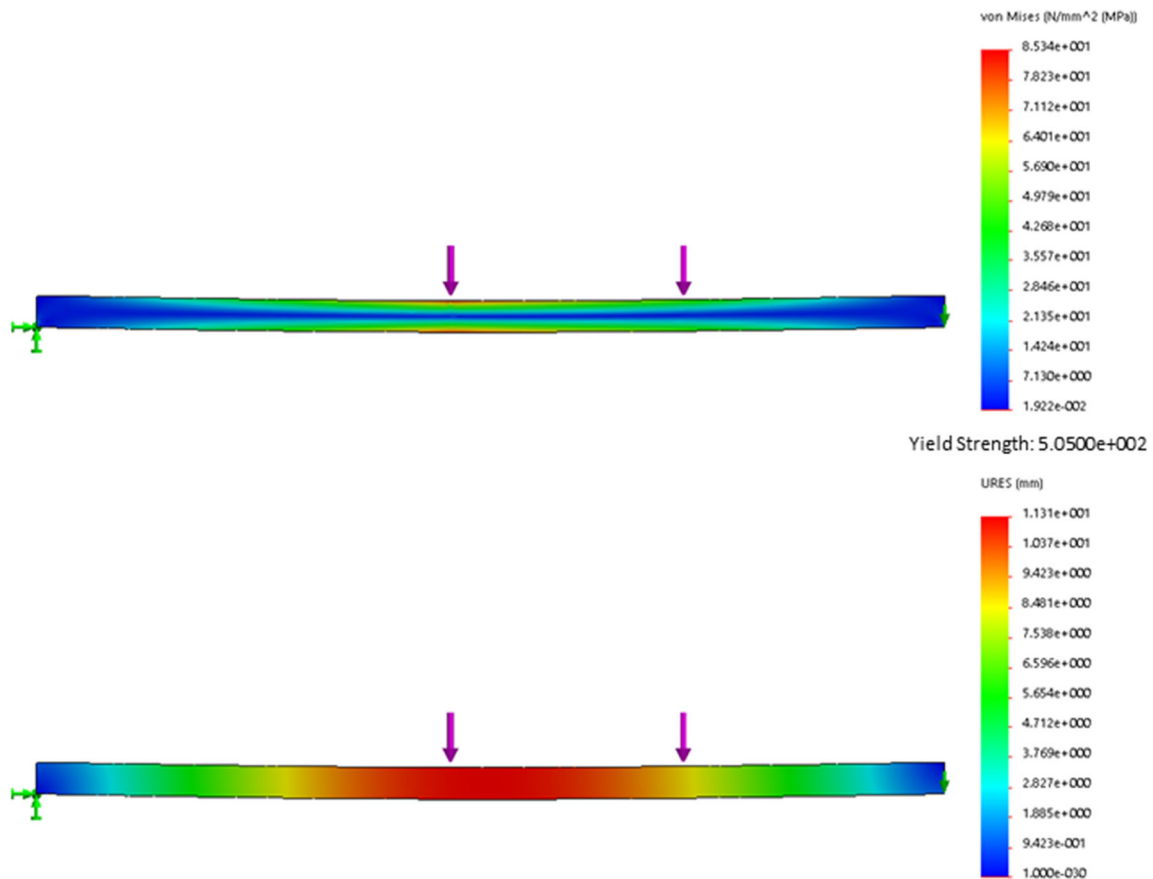


Figure 24. Stress and deflection analysis for Al 7075-T6.

Table 6. Deflection and factor of safety (FOS) analysis.

| Method | Max Deflection (mm) | Max Stress (MPa) | FOS |
|-------------------------|---------------------|------------------|------|
| <i>Al 6061 - T6</i> | | | |
| Analytical | – 11.77 | 80.95 | 3.41 |
| Finite Element Analysis | – 11.82 | 85.34 | 3.23 |
| <i>Al 7075 - T6</i> | | | |
| Analytical | – 11.31 | 80.95 | 6.21 |
| Finite Element Analysis | – 11.31 | 85.34 | 5.92 |

as in figure 21, the loads applied at B and C represents a singularity in the beam loading. This singularity results in discontinuities in the shear force V and bending moment M and requires use of different analytical functions to represent V and M in different portions of the beam. The use of singularity functions makes it possible to represent the shear force, the bending moment or the deflection in a beam by a single expression, valid at any point of the beam.

Singularity function of x is denoted by $\langle x - x_0 \rangle^n$, where n is any integer (positive or negative) including zero, and x_0 is a constant equal to the value of x at the beginning of a specific interval along the beam. Singularity function for $n \geq 0$ is partially defined as

$$\langle x - x_0 \rangle^n = \begin{cases} (x - x_0)^n & \text{for } x \geq x_0 \\ 0 & \text{for } x < x_0 \end{cases} \quad (14)$$

Integral and derivative of singularity functions are required for beam deflection problems. For $n > 0$

$$\int \langle x - x_0 \rangle^n dx = \frac{1}{n + 1} \langle x - x_0 \rangle^{n+1} + C \quad (15)$$

$$\frac{d}{dx} \langle x - x_0 \rangle^n = n \langle x - x_0 \rangle^{n-1} \quad (16)$$

For the beam in figure 22, the shear force and bending moment should be represented for 3 intervals: $0 \leq x \leq L_1$,

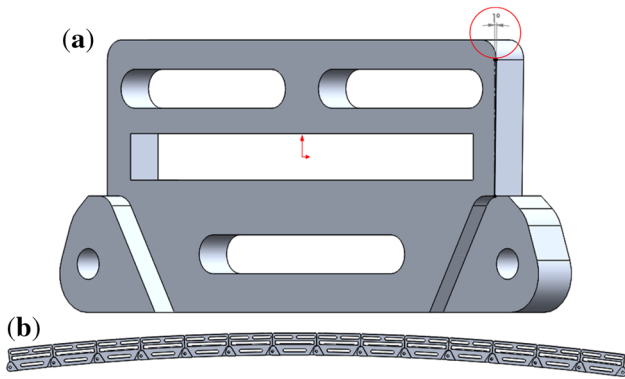


Figure 25. Side slope angle effect on curved chain.

$L_1 \leq x \leq L_2$ and $L_2 \leq x \leq L$. For these three intervals, the shear force and the bending moment can be represented using singularity functions as

Table 7. Comparing effect of the link with sharp edge and rounded edge.

| Angle between first two links | Diameter (mm) | |
|-------------------------------|-----------------|-----------|
| | Kinematic model | CAD model |
| 137° | 381.46 | 383.61 |
| 142° | 382.9 | 373.61 |

$$V(x) = F_{Ay} - F_{wheel}\langle x - L_1 \rangle^0 - F_{caster}\langle x - L_2 \rangle^0 \quad (17)$$

$$M(x) = F_{Ay}x - F_{wheel}\langle x - L_1 \rangle^1 - F_{caster}\langle x - L_2 \rangle^1 \quad (18)$$

Substituting $M(x)$ in Eq. (18) into Eq. (13) and integrating:

$$EIy = \frac{F_{Ay}}{6}x^3 - \frac{F_{wheel}}{6}\langle x - L_1 \rangle^3 - \frac{F_{caster}}{6}\langle x - L_2 \rangle^3 + C_1x + C_2 \quad (19)$$

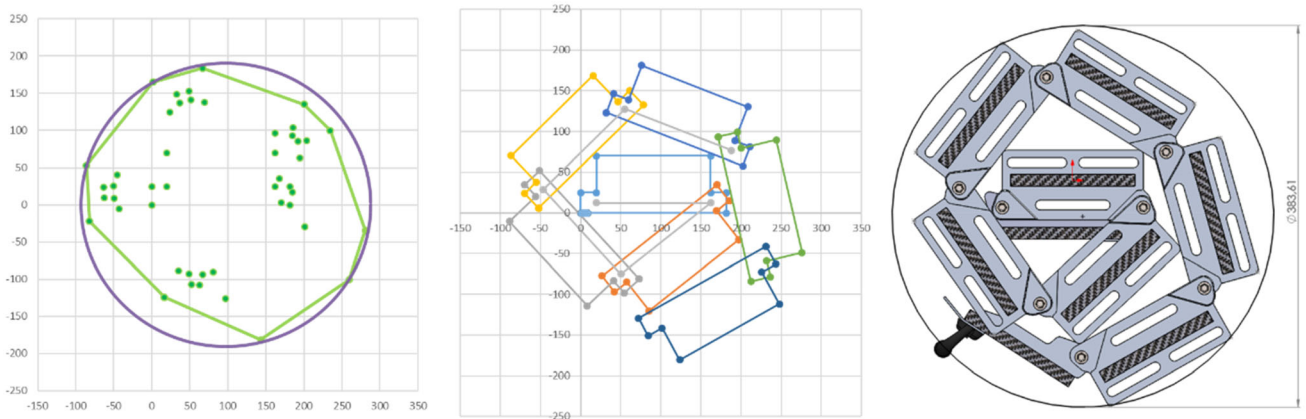


Figure 26. Effect of 137° rotation angle on compactness.

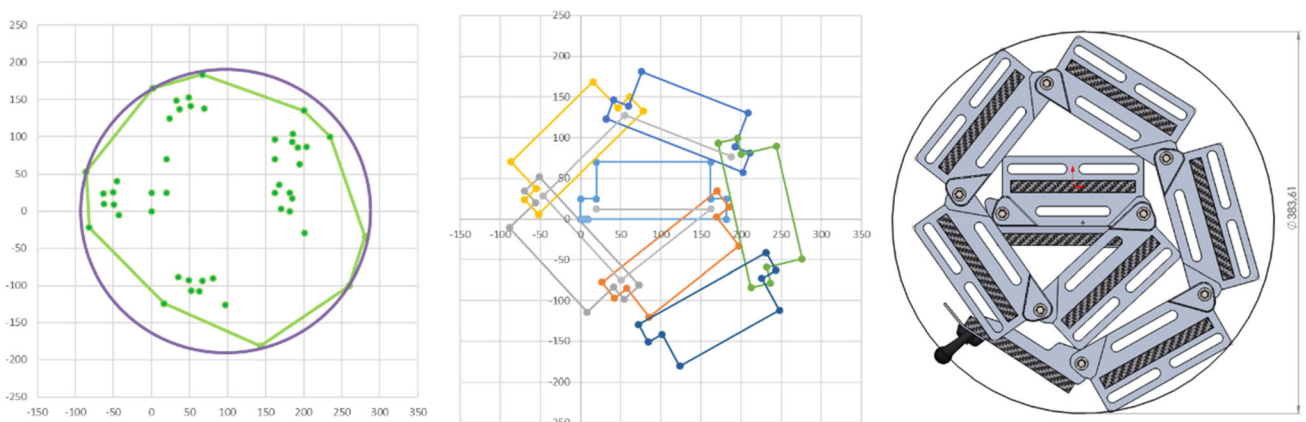


Figure 27. Effect of 142° rotation angle on compactness.

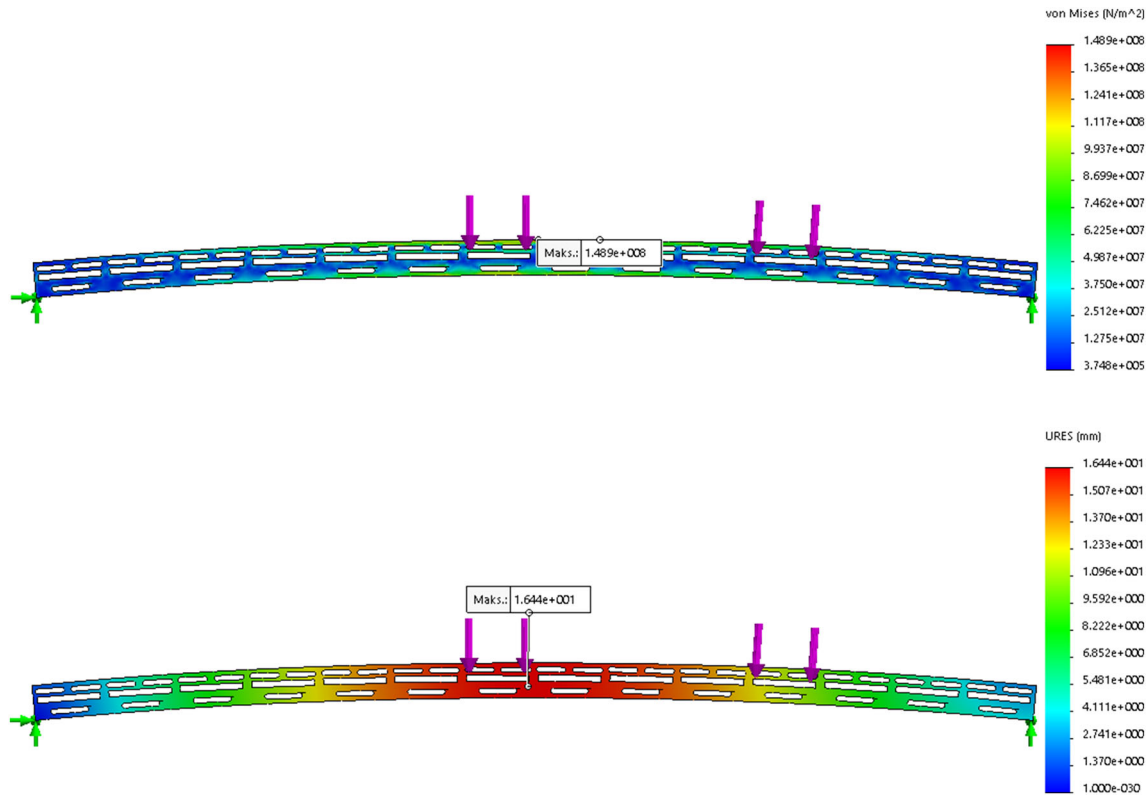


Figure 28. Stress and deflection analysis for Al 7075-T6, 1° slope.

Table 8. Deflection and FOS analysis of flat and curved beams.

| Slope Angle (°) | Max. Deflection (mm) | Max. Stress (MPa) | FOS |
|-----------------|----------------------|-------------------|------|
| <i>6061-T6</i> | | | |
| 0 | 17.4 | 148.7 | 1.86 |
| 0.5 | 17.4 | 148.3 | 1.86 |
| 1 | 17.1 | 148.9 | 1.85 |
| <i>7075-T6</i> | | | |
| 0 | 16.7 | 148.7 | 3.40 |
| 0.5 | 16.7 | 148.3 | 3.41 |
| 1 | 16.4 | 148.9 | 3.39 |

The constants C_1 and C_2 can be determined from the boundary conditions: $y = 0$ at $x = 0$ and $x = L$:

$$C_1 = \frac{F_{wheel}(L - L_1)^3 + F_{caster}(L - L_2)^3 - F_{Ay}L^3}{6L} \quad (20)$$

$$C_2 = 0$$

The first step is determining the position of the maximum deflection, by using singularity function, which depends on design parameters (table 5) and the free body diagram of the wheelchair (figure 21). The formulations are implemented in Excel to find the position of wheelchair which causes the maximum deflection by increasing x value gradually. The results of analytical integration

(Eq. (20)) are crosschecked with numerical integration using finite differences. Shear force, bending moment and deflection diagrams of the simply supported beam representing one side of the ramp are illustrated in figures 22-23.

According to the computations, maximum deflection occurs at 991 mm where the back wheel is at 910 mm. Finite element analysis is also conducted using SolidWorks to verify this result which is used during structural design. The stress and deflection variation for Al 7075-T6 are depicted in figure 24 (the variations are similar for Al 6061-T6). The results are compared in table 6.

The maximum deflection is found as -11.82 mm for Al 6061-T6 and -11.31 mm for Al 7075 T6 while the factor of safety (FOS) is 3.32 and 5.91 respectively according to finite element analysis (figure 24, table 6). The expected FOS is 2, thus the general structural measurements (thickness, height) are quite enough for the structural design of the links to reduce weight. Moreover, maximum deflection values can be decreased and made nonnegative by designing an arch-like curved structure instead of a flat beam.

3.4 Structural design

For structural design, only one side of the ramp is subjected to analysis for simplifying the finite element

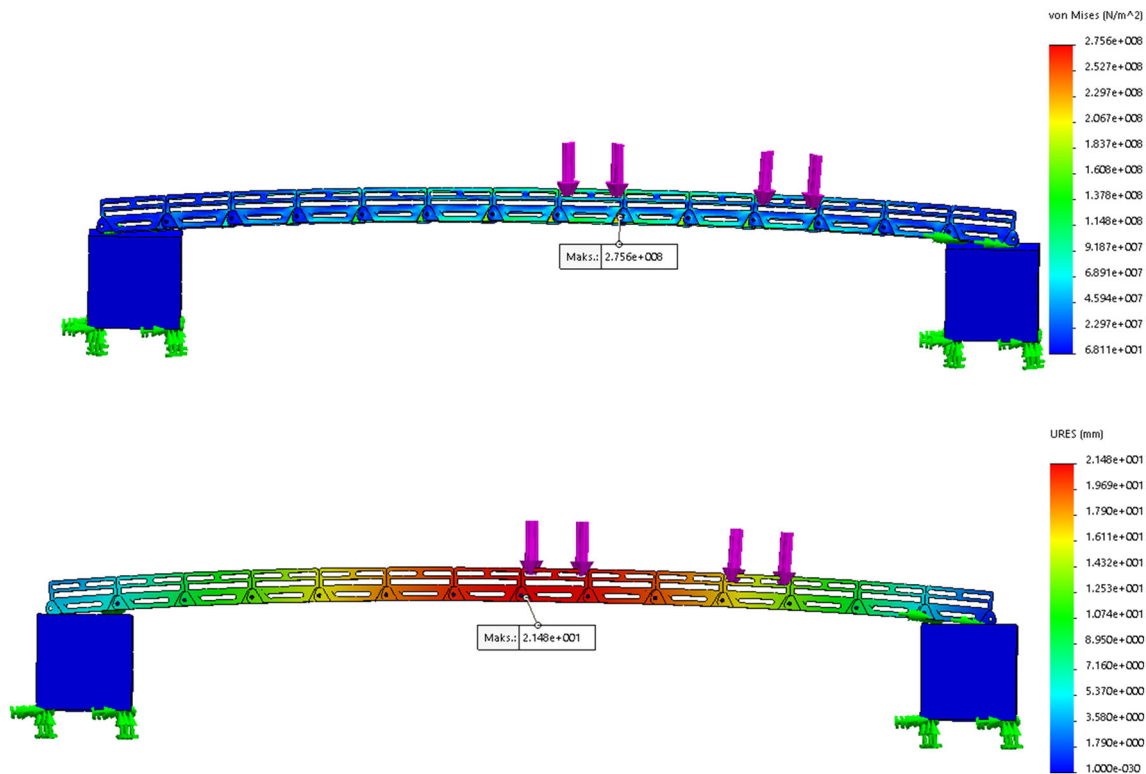


Figure 29. Stress and deflection analysis of link chain for Al 7075-T6, 1° slope angle.

analysis. Curved link chains are generated by creating 0° , 0.5° and 1° slope angle at the sides of the links that creates a curved structure to prevent negative deflection in the deployed form (figure 25). Also, the sharp edges are rounded for decreasing the possible stress concentrations and preventing physical injuries. This small modification makes a slight difference for the compact rolled form of the ramp (figures 26-27). As can be seen from table 7, kinematic and CAD models' diameters are slightly different and most compact configuration for CAD model forms when the angle between first two links is 142° .

The curved link chains are represented as simply supported curved beams. Structural design is performed by removing redundant material from where the stress occurs less due to loading conditions. The simulation is performed based on the boundary conditions which represents the extreme loading conditions. To this end, link chain is positioned parallel to the ground and loaded according to defined conditions in Section 3.3.3. As a sample of the simulation results, stress and deflection variation for Al 7075-T6, 1° slope is presented in figure 28.

Redundant material pattern, where the blanks are introduced, is determined due to assembly areas where the composite panels, hand rails and telescopic legs may be assembled. Stress distribution is observed whether redundant materials cause to exceed yield point or not. Numerical results are summarized in table 8.

Table 8 shows that the small curvature for the single-piece beam has no significant effect on deflection and FOS. This is because the radius of curvature is large enough to be neglected and Eq. (19) is valid. A curved beam can be treated as a flat beam if the radius of curvature is greater than 10 times the depth of the beam's cross section [36]. However, the curved assembly load-bearing members may not behave the same as the single-piece beam in real case. Therefore, assembly analyses are performed for 0° and 1° slope angles for Al 7075-T6 by selecting no penetration contact type and using soft springs to stabilize the model for simulating the real loading conditions (figure 29, table 9).

According to the finite element analysis results, curved structures create horizontal reaction forces unlike a flat beam, thus it is expected that the load-bearing capacity increases and deflection decreases. Even though the structure is slightly curved, this result can be observed in table 9. Curved design is also preferred to prevent negative deflections under the level of the supports.

3.5 Deflection of a simply-supported sandwich beam with antiplane core and thin faces

The stresses and deflections in a sandwich beam as shown in figure 30 may be approximately found using the theory of bending presented in Section 3.3.2. An

Table 9. Deflection and FOS Analysis of flat and curved link chains.

| Slope Angle (°) | Max. Deflection (mm) | Max. Stress (MPa) | FOS |
|-------------------|----------------------|-------------------|------|
| <i>Al 7075-T6</i> | | | |
| 0 | 25.95 | 245.9 | 2.05 |
| 1 | 21.48 | 242.9 | 2.08 |

antiplane core is an idealized core in which the modulus of elasticity in planes parallel with the faces is zero but the shear modulus in planes perpendicular to the faces is finite. A honeycomb core can be considered an antiplane core and by this definition $E_c = 0$ and the antiplane core makes no contribution to the bending stiffness of the beam [37].

The sandwich beam illustrated in figure 31 consists of two thin faces each of thickness t , separated by a thick

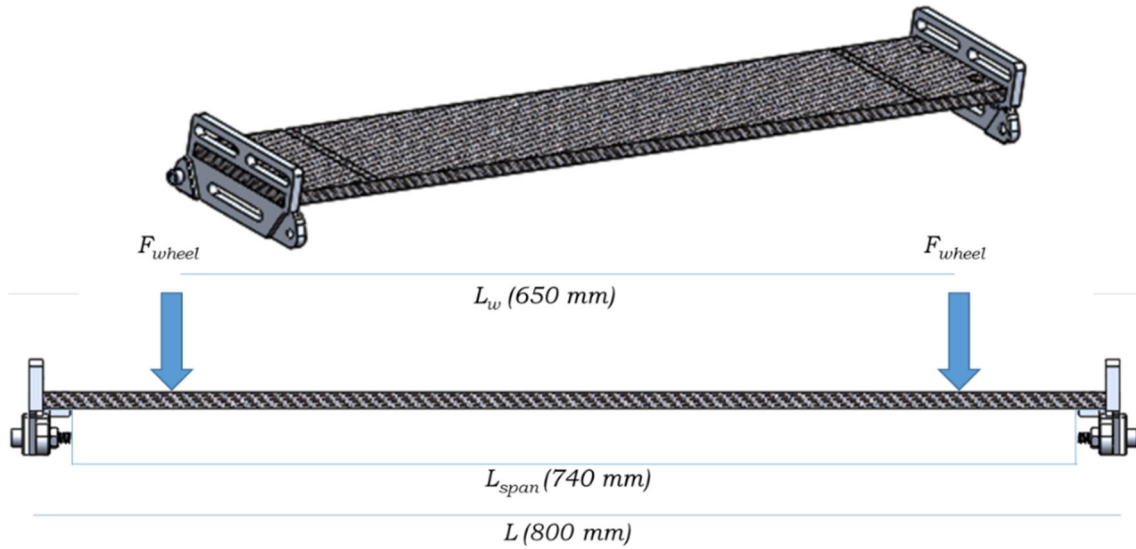


Figure 30. Sandwich composite panel loading conditions.

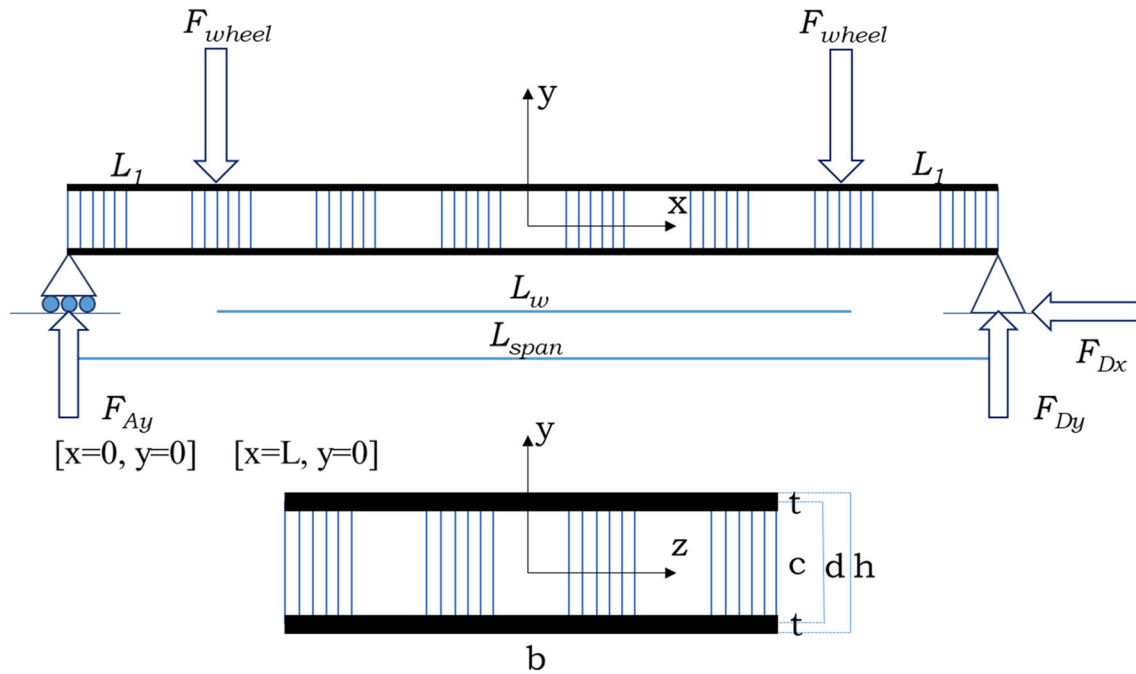


Figure 31. Determining the maximum deflection of the simply supported sandwich beam.

Table 10. Design parameters for sandwich composite beam with 10 mm-thick Al honeycomb core.

| | |
|-----------------|-------|
| L_{span} (mm) | 740 |
| L_w (mm) | 650 |
| F_{wheel} (N) | 1175 |
| b (mm) | 125 |
| c (mm) | 10 |
| t (mm) | 1.43 |
| d (mm) | 12.85 |

core, of low density material of thickness c . The overall thickness of the beam is d and the width is b . All three layers are firmly bonded together and the face material is much stiffer than the core material. It is assumed that the face and core materials are both isotropic.

It is convenient to denote the flexural rigidity EI by D . The sandwich beam in figure 31 is a composite beam, so its flexural rigidity is the sum of the flexural rigidities of the two separate parts, faces and core, measured about the neutral axis of the entire cross-section [37]. However, the flexural rigidity of the core material generally provides no stiffness ($E_f \gg E_c$ where E_f and E_c are the moduli of elasticity of the faces and core respectively). Thus, the influence of flexural rigidity of the core can be neglected [38].

$$D = E_f \frac{(d^3 - c^3)b}{12} \text{ (N} \cdot \text{mm}^2) \tag{21}$$

Panel shear rigidity:

$$U = \frac{G(d + c)^2 b}{4c} \text{ (N)} \tag{22}$$

where G is core shear modulus in MPa. The stresses in the faces and core may be determined using bending theory adapted to the composite nature of the cross-section.

$$\sigma_f = \frac{My}{D} E_f \left(\frac{c}{2} \leq y \leq \frac{d}{2}; -\frac{d}{2} \leq y \leq -\frac{c}{2} \right) \tag{23}$$

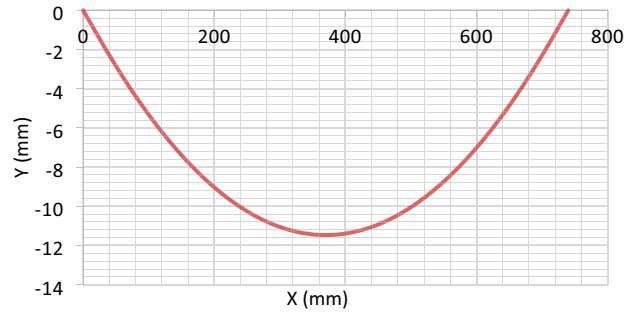
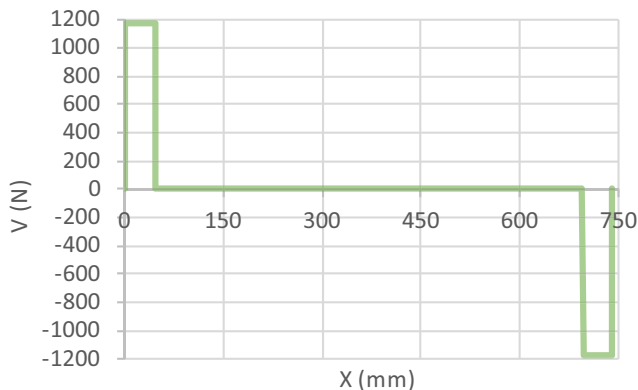


Figure 33. Deflection diagram of composite panel.

Table 11. Loading conditions, material properties and deflection values for the composite panel.

| | |
|------------------------------------|-----------|
| P (N) | 1175 |
| U (N) | 275745.95 |
| D (N·mm ²) | 314020502 |
| Bending Ultimate Strength (MPa) | 118.307 |
| Core Ultimate Shear Strength (MPa) | 0.76 |
| Face Bending Stress (MPa) | 13.00 |
| FOS for bending stress | 9.1 |
| Core Shear Stress (MPa) | 0.41 |
| FOS for Shear Stress (MPa) | 1.85 |
| y_{max} (mm) | -11.46 |

$$\sigma_c = \frac{My}{D} E_c \left(-\frac{c}{2} \leq y \leq \frac{c}{2} \right) \tag{24}$$

As expected the maximum face and core stresses are obtained while $y = \pm d/2$ and $y = \pm c/2$ respectively. The assumptions of the theory of bending lead to Eq. (23) for the shear stress, τ , in a homogeneous beam at a depth y , below the centroid of the cross-section:

$$\tau = \frac{P}{(d + c)b} \tag{25}$$

where P is the shear force at the section under

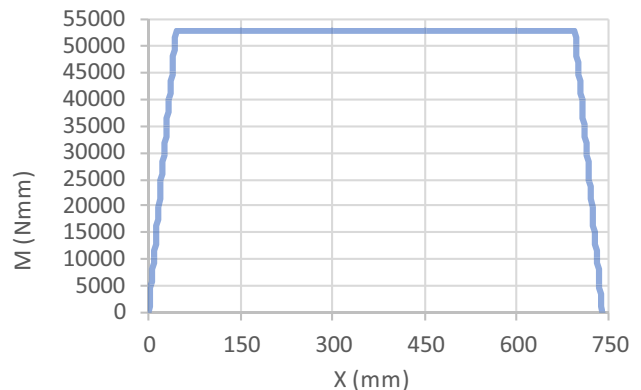


Figure 32. Shear force and bending moment diagrams of composite panel.



Figure 34. First full-scaled prototype.

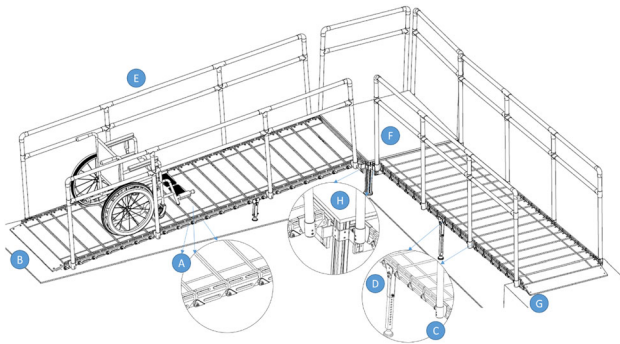


Figure 35. Assembling and positioning [13].

Table 12. Components of the ramp assembly.

| | |
|---|---|
| A | Panels |
| B | Approach Plate |
| C | Handrail's Mounting Bracket |
| D | Telescopic Legs |
| E | Handrails |
| F | Rotation Platform |
| G | Positioning of the First Module on a Flat Surface |
| H | Ramp Mounting Bracket |

consideration. Sandwich panel deflection for four-point load, one-quarter span according to ASTM C-393 is as follows:

$$\Delta = \Delta_1 + \Delta_2 = \frac{11PL^3}{768D} + \frac{PL}{8U} \quad (26)$$

For a simply supported beam, shear deflection (Δ_2) is usually ignored because it has a very small effect on entire deflection compared to bending deflection (Δ_1). The central shear deflection of a sandwich composite beam can be calculated as $\frac{PL}{8U}$ where the bending moment at the center is

$\frac{PL}{8}$ and U is the panel shear rigidity. The loading conditions on the sandwich panel are illustrated in figure 31 and the necessary numerical data are given in table 10.

Force equilibrium for the sandwich panel results in $F_{Ay} = F_{Dy} = F_{wheel} = P$. Similar to Eq. (19), the deflection curve of the sandwich panel can be expressed as

$$Dy = \frac{P}{6} \left[(x^2 - L^2)x - (x - L_1)^3 - (x - (L - L_1))^3 + \frac{(L - L_1)^3 + L_1^3}{L}x \right] \quad (27)$$

Due to the symmetrical loading conditions on the panel, the maximum deflection occurs at the middle $x = L/2$ where the deflection is given by

$$Dy = \frac{P}{6} \left[(x^2 - L^2)x - (x - L_1)^3 + \frac{(L - L_1)^3 + L_1^3}{L}x \right] = \frac{PL_1}{6} (3x^2 - 3Lx + L_1^2) \quad (28)$$

The shear force, bending moment and deflection diagrams are presented in figures 32-33. The numerical data are summarized in table 11.

Factor of safety according to face bending stress is found as 9.1. However, sandwich beam's FOS should be determined according to core ultimate shear stress, because core gets damaged before face fracture occurs due to real loading conditions. FOS for shear stress is 1.85. However, FOS can be increased by increasing core thickness, face thickness and/or panel width or by using smaller cell sized Al honeycomb. limitations can be listed as:

- Core material cell size and thickness can be customized if there is a wholesale demand.
- Face thickness can be increased. This is an expensive solution and causes increasing total weight.

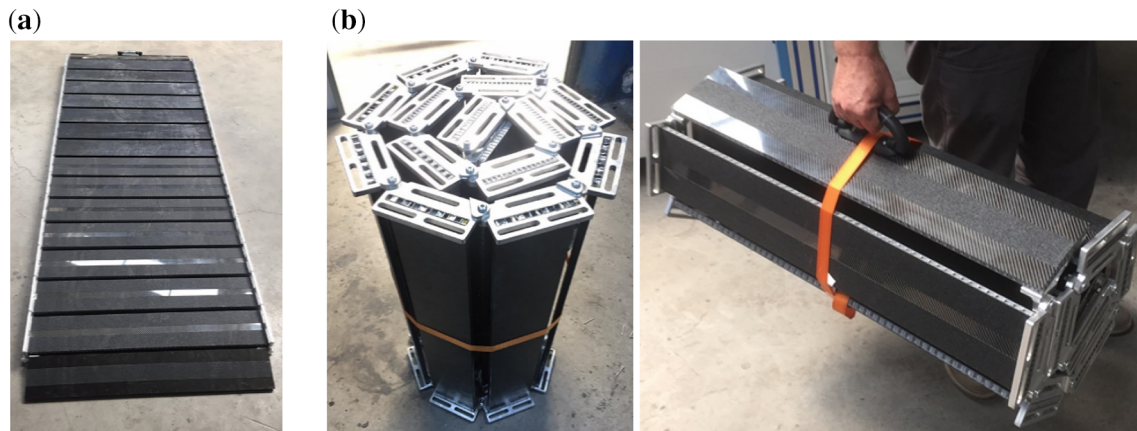


Figure 36. (A) 2 m ramp assembly in deployed form, (B) 1 m (half of) ramp in rolled form [13].



Figure 37. Load tests.

- Panel width is restricted by link length.

4. Prototype and tests

Final prototype is manufactured step-by-step. Design verification of the prototype is conducted by testing the ramp under overloading conditions. Moreover, the field tests are also performed with 7 wheelchair users who have been using wheelchair at least for 1 year in order to ask their opinions and suggestions about prototype.

4.1 First full-scaled prototype

Ramp links are 3D printed with PLA filament to prevent possible design errors in terms of rolling and assembling ability (figure 34). Geometric tolerances are found to be fairly good for centering and assembling the connection axes providing rolling ability.

4.2 Final design and prototype

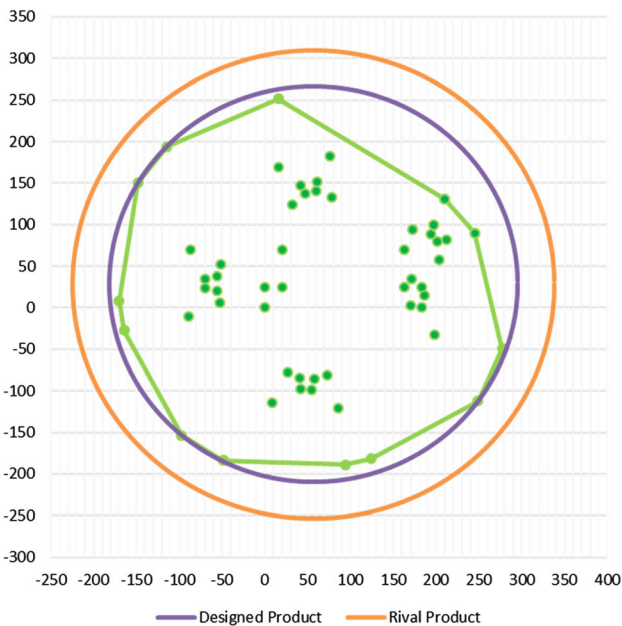
Final assembly is modeled in SolidWorks after geometric and strength calculations are completed. A gradual ramp design is aimed as suggested by Sangelkar and McAdams [39]. Handrails and telescopic legs may be assembled in case of requirement where the redundant materials are removed (figure 35, table 12). Ramp length can be extended by adding modules. The whole structure should be supported by telescopic legs at every 14 module.

4.3 Manufacturing

First, ramp links and composite panels are manufactured. Then modules are formed by assembling two consecutive links with a composite panel. Then modules are assembled together to create a rollable ramp chain. Finally, approach plates are assembled to each ends of the ramp to avoid elevation difference between ground and the ramp. Ramp links are manufactured with a CNC milling machine. Then, burrs are removed with various hand tools such as riffler, dremel and sandpapers. Geometric tolerances are controlled by assembling the links through their connection holes, before assembling the module. Manufacturing process for sandwich composite panel starts with manufacturing carbon fiber face sheets with vacuum infusion technique. Then, two face sheets are bonded with a 10 mm-thick aluminum honeycomb core with an epoxy



Figure 38. Field test with wheelchair users [13].



| | Rival Product | Designed Product |
|-------------------------|---------------|------------------|
| Diameter (mm) for 1,5 m | 563 | 476,24 |
| Weight per meter (kg) | 7,78 | 6,31 |

Figure 39. Comparison of the best rival and designed product.

adhesive and cured under vacuum pressure. To prevent core-face separation, sandwich panels are cut with a CNC router machine according to design measurements and covered with one layer of pre-preg and cured again with vacuum pressure.

Modules are formed by assembling 2 aluminum links with a composite panel. First, composite panel is bonded to a link with an epoxy adhesive to prevent clearance between assembling gap on the link and composite panel. Then rivets are used for securing the connection. Modules are assembled together to create the rollable ramp chain. Each module in assembly is able to rotate about their connection axes (figure 36).

Approach plates are designed in order to make elevation difference between ground and ramp zero (can be seen in figure 36a). The approach links are manufactured with a CNC milling machine, while the approach plate material is the same material as the load-bearing panels. Approach plates are bonded to approach links. Then the plates are assembled to each ends of the ramp. To avoid the slight elevation difference between the ground and approach plates, an aluminum sheet is bended and bonded at the end of the plate. Also a handle is assembled to the approach plates for easy carrying.

4.4 Load and field tests

Design verification of prototype is conducted by testing the ramp structure under the predetermined loading conditions. Firstly, ramp is loaded with 543 kg (figure 37), which is nearly two times greater than ramp's determined loading capacity (300 kg / (2 m)). Then, the field test is performed with 7 wheelchair users who have been using wheelchair at least for 1 year (figure 38).

Users' opinions and suggestions about the prototype are taken during field test in terms of ramp width, load-bearing capacity, anti-slip surface sufficiency and efficiency. All of the participants indicated that anti-slip surface of the ramp

is much more effective than any other fixed public ramps. Four of the participants found the ramp quite wide due to their narrower wheelchairs, and suggested that a narrower ramp may be more effective. All of the participants found the design practical to use in their daily life and claimed that they may purchase one. Two of the participants had their family members during field test and their opinions are also taken. Family members gave feedback about the general design, ease of use, weight and ease of storage and possible place of use. All feedbacks are positive in terms of satisfying users' expectations. One of the family members suggested that the ramp may not only be used for outdoor but also can be used for indoor such as shower stall.

5. Conclusions

In this study, the design of a temporary ramp for wheelchair users is presented. The designed rollable ramp consists of serial chain members which are able to rotate about the connection axes. Geometrical calculations are conducted for achieving a better compactness while the ramp is in rolled form. In accordance with this purpose, several geometric patterns of ramp links are modeled both in SolidWorks and Excel with the help of convex hull and smallest enclosing circle algorithms to find optimal link length and shapes. Strength calculations are conducted for a simply supported beam model for determining height and thickness of the links. Then, blanks are designed in SolidWorks to make the link structure lighter. The designed ramp is 15.4% more compact and has 18.87% less weight compared to the best rival product available in the market that has least weight and most compact (figure 39). At the end of the study, field test is performed to get user opinions and suggestions about the new design.

Acknowledgements

This work was funded by The Scientific and Technological Research Council of Turkey (TÜBİTAK) (1512-Entrepreneurship Multi-phase Programme) with grant no. 2150530 and conducted within the scope of a MSc thesis in the Department of Mechanical Engineering, İzmir Institute of Technology. The authors are grateful to Prof. Bülent Yardımoğlu and Prof. Metin Tanoğlu for sharing their knowledge during structural design and experimental stage of this work.

References

- [1] Matsuoka Y, Kawai K and Sato R 2003 Vibration simulation model of passenger-wheelchair system in wheelchair-accessible vehicle. *ASME J. Mech. Des.* 125(4): 779–785
- [2] Justak J 2013 *Telescoping and Magnetic Tailgate Ramp*. U.S. Patent No. 20130028693
- [3] Breslin P W and Shoen M V 1998 *Telescoping Truck Loading Ramp Assembly*. U.S. Patent No. 5813071
- [4] Boone F J 1994 *Tailgate Enclosed Telescopic Ramp Structure*. U.S. Patent No. 5312149
- [5] Carter C D 2011 *Multi Tread Segmented Self-Deploying Roll Up Ramp*. U.S. Patent No. 7958586
- [6] Aulicino K M 2006 *Roll Up Ramp System*. U.S. Patent No. 20060214456
- [7] Kenville T E, Schmaltz D and Stanislawo J 2003 *Loading Ramp Device Which Rolls Up for Convenient Storage*. U.S. Patent No. 6643878
- [8] Kenville T E, Schmaltz D and Stanislawo J 2002 *Loading Ramp Device Which Rolls Up for Storage*. U.S. Patent No. 20020088065
- [9] Martinez J 2002 *Portable Ramp with Transport Facilitators*. U.S. Patent No. 20020108190
- [10] Campbell P L 2009 *Portable Wheelchair Ramp*. U.S. Patent No. 20090300860
- [11] Jones R P 2002 *Stowable Load Ramp for Vehicles*. U.S. Patent No. 6378927
- [12] Kenny M 2011 *Extendable Ramp for Storage in a Tailgate or Flat Bed*. U.S. Patent No. 20110072596
- [13] Doğan Kumtepe E, Başoğlu A N, Çorbacioğlu E, Daim T U and Shaygan A 2020 A smart mass customization design tool: a case study of a portable ramp for wheelchair users. *Health Technol.* 10: 723–737
- [14] Sheldon S and Jacobs N A 2006 *Report of a Consensus Conference on Wheelchairs for Developing Countries*. Bengaluru, India
- [15] Frost K L, Bertocci G and Smalley C 2015 Ramp-related incidents involving wheeled mobility device users during transit bus boarding/alighting. *Arch. Phys. Med. Rehabil.* 96: 928–933
- [16] Silva N, Kanuwana N, Bandara P, Jayalath S, Mendis R and Costa S 2015 Assessment of the suitability of ramps for wheel chair access among public buildings in Colombo Sri Lanka. *Physiotherapy* 101: eS719–eS720
- [17] Kim C S, Lee D, Kwon S and Chung M K 2014 Effects of ramp slope, ramp height and users' pushing force on performance, muscular activity and subjective ratings during wheelchair driving on a ramp. *Int. J. Ind. Ergon.* 44: 636–646
- [18] Meyers A R, Anderson J J, Miller D R, Shipp K and Hoenig H 2002 Barriers, facilitators, and access for wheelchair users: substantive and methodologic lessons from a pilot study of environmental effects. *Soc. Sci. Med.* 55: 1435–1446
- [19] Brown T 2009 *Change by Design: How Design Thinking Transforms Organizations and Inspires Innovation*. Harper Business, New York, NY
- [20] Mootee I 2013 *Design Thinking for Strategic Innovation: What They Can't Teach You at Business or Design School*. John Wiley & Sons, Hoboken, NJ, pp 16–69
- [21] Ambrose G and Harris P 2010 *Design Thinking*. AVA Publishing, Lausanne
- [22] Berg M, Cheong O, Kreveld M and Overmars M 2008 *Computational Geometry, Algorithms and Applications*. Springer-Verlag, Berlin, pp 1–8
- [23] Jarvis R 1973 On the identification of the convex hull of a finite set of points in the plane. *Inf. Process. Lett.* 2: 18–21
- [24] Skyum S 1991 A simple algorithm for computing the smallest enclosing circle. *Inf. Process. Lett.* 37: 121–125

- [25] Askeland D R and Phule P P 2006 *The Science and Engineering of Materials*. 5th edn. Thomson, London, pp 402–411
- [26] Songmene V, Djebara A, Zaghbani I, Kouam J and Khettabi R 2011 Machining and machinability of aluminum alloys. In: *Aluminium Alloys, Theory and Applications* (ed) Kvackaj T, Rijeka, InTech, pp 377–398
- [27] Rana R S, Purohit R and Das S 2012 Reviews on the influences of alloying elements on the microstructure and mechanical properties of aluminum alloys and aluminum alloy composites. *Int. J. Sci. Res. Publ.* 2: 1–7
- [28] Kaufman J G 2000 *Introduction to Aluminum Alloys and Tempers*. ASM International, Materials Park, OH, pp 9–22
- [29] Carlsson L A and Kardomateas G A 2011 *Structural and Failure Mechanics of Sandwich Composites*. Springer, Dordrecht
- [30] Beer F P, Johnston E R and DeWolf J T 2001 *Mechanics of Materials*. 3rd edn. McGraw-Hill, New York, NY
- [31] Ashby M F 2005 *Materials Selection in Mechanical Design*. Elsevier Butterworth-Heinemann, Oxford
- [32] Daniel I M and Abot J L 2000 Fabrication, testing and analysis of composite sandwich beams. *Compos. Sci. Technol.* 60: 2455–2463
- [33] 1800wheelchair.com 2017 *Heavy Duty Power Wheelchairs*. accessed June 5, 2017, <http://www.1800wheelchair.com/category/heavy-duty-power-chairs>
- [34] Mathew D 2016 *Wheelchair*. last modified March 22, 2016, <https://grabcad.com/library/wheelchair-18>
- [35] Winter A and Hotchkiss R 2007 *Mechanical Principles of Wheelchair Design*. MIT Manual, last modified August 14, 2007, <http://web.mit.edu/awinter/Public/Wheelchair/Wheelchair%20Manual-Final.pdf>
- [36] Young W C, Budynas R G and Sadegh A M 2012 *Roark's Formulas for Stress and Strain*. 8th edn. McGraw-Hill, NY
- [37] Allen H G 1969 *Analysis and Design of Structural Sandwich Panels*. Pergamon Press, London
- [38] Phang M K S and Kraus H 1972 Flexural behavior of reinforced-concrete sandwich composites. *Exp. Mech.* 12: 549–556
- [39] Sangelkar S and McAdams D A 2012 Adapting ADA architectural design knowledge for universal product design using association rule mining: a function based approach. *ASME J. Mech. Des.* 134: 071003